NASA Technical Paper 1405

Near-Field Sonic-Boom Pressure Signatures for the Space Shuttle Launch and Orbiter Vehicles at Mach 6

George C. Ashby, Jr.

APRIL 1979

NASA

NASA Technical Paper 1405

Near-Field Sonic-Boom Pressure Signatures for the Space Shuttle Launch and Orbiter Vehicles at Mach 6

George C. Ashby, Jr.
Langley Research Center
Hampton, Virginia

National Aeronautics
and Space Administration

**Scientific and Technical
Information Office**

1979

SUMMARY

Static-pressure signatures parallel to the flight path of the launch and entry configurations of the space shuttle have been measured in the Langley 20-inch Mach 6 tunnel in air at selected distances from the flight path. The launch configuration, consisting of an equivalent body of revolution (representing the orbiter and external fuel tank) with a solid exhaust gas plume attached, was tested at an angle of attack of 0°. The entry configuration (orbiter only) was tested over an angle-of-attack range from 10° to 40°.

Results from the tests show that conventional static-pressure probes cannot be used in the vicinity of strong shocks but can be used when completely behind the shock; a pitot probe gives more accurate values at the shock. This observation is reinforced by the agreement between the peak overpressure calculated from a finite-difference method and the value obtained from the pitot-pressure measurement.

The areas under the calculated pressure signatures were found to be in good agreement with those under the measured signatures for the launch configuration at an angle of attack of 0° and for the entry configuration at angles of attack of 25° and 30°. These excellent predictions of signature areas and peak overpressures show that theoretical estimates are acceptable as initial conditions for extrapolation to ground level to establish the intensity of the resulting sonic boom. Wind-tunnel measurements would be needed only on a limited basis to verify the results.

INTRODUCTION

Sonic-boom overpressures generated by the space shuttle during ascent and orbiter entry are under investigation because extensive land areas may be affected. The shuttle operational flight envelopes are far outside those associated with sonic-boom predictions for aircraft, and overpressures may be much more severe. The values of the governing parameters - Mach number, altitude, angle of attack, flight-path angle, bank angle, and linear and angular acceleration rates have much greater ranges for the shuttle than for configurations previously investigated in sonic-boom research (ref. 1). In addition, the shuttle sonic boom generated during ascent involves shock waves from large exhaust gas plumes. For these extreme flight conditions, specialized methods of predicting sonic-boom overpressures from near-field pressure signatures have been developed (refs. 2 and 3).[1]

---

[1]A simplified method, based on far-field pressure signatures, for predicting the sonic boom from a wide variety of supersonic aircraft and spacecraft was developed and verified in references 4 and 5, respectively.

These techniques were used to predict the sonic-boom characteristics for the launch and entry configurations of Apollo 15, 16, and 17 (refs. 1, 6, and 7). Using wind-tunnel pressure signatures, the predictions agreed very well with flight measurements. These techniques were also used to make the initial estimates of the sonic-boom characteristics for the early shuttle launch and entry configurations. With the evolvement of the shuttle configurations, near-field pressure signatures were needed to define the sonic-boom parameters of the final system. Towards that end, pressure signatures for the space shuttle launch configuration with and without simulated exhaust gas plumes were presented in reference 8 at Mach numbers from 3.0 to 5.54, and for the orbiter at Mach numbers from 1.3 to 4.0 in reference 9.

The current study was conducted in support of the overall sonic-boom evaluation for shuttle operations. In particular, the strong-shock near-field pressure signatures associated with the exhaust gas plume for the launch configuration (ref. 8) and with high angles of attack for the entry configuration (ref. 9) have been obtained at Mach 6. These data update and expand the base for defining the sonic-boom parameters of the final shuttle system.

This report presents the static-pressure signatures obtained from pitot- and static-probe traverses along a line parallel to the flight path with models at appropriate angles of attack and various roll angles. Theoretical predictions of the pressure signatures are compared with experimental results.

SYMBOLS

h	distance from flight path to pressure probes, mm
l	reference length of configuration, mm (see fig. 1)
M_2	Mach number behind bow shock
M_∞	free-stream Mach number
p	local static presure, Pa
Δp	sonic-boom overpressure, $p - p_\infty$, Pa
$p_{t,2}$	total pressure behind bow shock, Pa
$p_{t,3}$	pitot pressure behind bow shock, Pa
$p_{t,\infty}$	free-stream total pressure, Pa
$p'_{t,\infty}$	free-stream pitot pressure, Pa
p_2	static pressure behind bow shock, Pa
p_∞	free-stream static pressure, Pa

x location of traverse points from reference, mm (see sketches at top of tables I and II)

Δx distance along abscissa of pressure signature from adjusted origin, mm

α angle of attack, deg

θ shock-wave angle, deg

ϕ meridional or roll angle, deg

APPARATUS AND TESTS

Tunnel

The tests were conducted in the Langley 20-inch Mach 6 tunnel at an average stagnation pressure of 2.86 MPa and an average stagnation temperature of 494 K. Operational characteristics of the facility and the flow calibration are presented in reference 10.

Models

The two models used in the test program are shown in figure 1. Figure 1(a) shows a 0.000456-scale model of a configuration representative of the space shuttle with its dominating exhaust gas plume during ascent at Mach 6. Because the orbiter and its attached external fuel tank are of minor importance compared with the exhaust gas plume, they are represented in the model by an equivalent body which has the same cross-sectional area distribution. The simulated plume body represents the area distribution of the gaseous exhaust plume plus the mixing region between the plume inner shock and the external flow. Its shape and size were determined in the manner described in reference 7.

A detailed 0.0041-scale model of the orbiter configuration, designated 089B by Rockwell International, is shown in figure 1(b).

Instrumentation

Electrical transducers were used to sense the pressures, and a digital shaft encoder was used to identify the position of the probes in the flow field. The static-pressure probe (fig. 2) had three pairs of orifices. One pair was positioned so that the orifices were diametrically opposed with their axis normal to the probe longitudinal axis. The other two pairs of orifices, whose axes lie on a plane normal to the axis of the single pair, were drilled at 25° and 35° relative to the probe longitudinal axis. A probe with an orifice axis slanted in the same direction as the shock was expected to measure the pressure rise at the shock more accurately than a probe with the orifice axes all normal to the probe longitudinal axis. The pitot-pressure probe (fig. 2) had an internal bevel to reduce the probe sensitivity to flow angle.

Tests and Methods

The static-pressure and pitot-pressure probes were mounted beside each other at the same radius from the model reference axis and were separated according to their respective shock angles to avoid mutual interference (fig. 3). Pitot-pressure and static-pressure measurements were made at stations from in front of the bow shock to the downstream limit of the traverse apparatus for each run, the probes were set in the most forward survey position at the distance h from the reference axis. The model was positioned longitudinally so that the bow shock was slightly aft of the orifices of both probes. At the beginning of each run, the probes were moved aft until the beginning of the sharp pressure increase at the shock was encountered. Then the probes were moved forward of the shock and the data traverse across the shock was begun. Discrete data points were taken over the allowable traverse distance with multiple data points being taken in the vicinity of maximum overpressure to define that particular point as accurately as possible. Traverses were made in both directions over the allowable traverse distance.

The launch configuration was tested at an angle of attack of 0° at several meridional angles. The orbiter was tested over an angle-of-attack range from 10° to 40° at several meridional angles.

DATA REDUCTION

The free-stream Mach number (M_∞) and static pressure (p_∞) were obtained by using $p'_{t,\infty}$ from the floor-mounted pitot probe and the free-stream total pressure ($p_{t,\infty}$). The static-pressure signatures from the static-pressure probe were obtained directly, but those from the pitot probe were calculated iteratively with the following equations (ref. 11):

From oblique-shock relationships,

$$\frac{p_{t,2}}{p_{t,\infty}} = \left(\frac{6M_\infty^2 \sin^2\theta}{M_\infty^2 \sin^2\theta + 5}\right)^{7/2} \left(\frac{6}{7M_\infty^2 \sin^2\theta - 1}\right)^{5/2} \tag{1}$$

$$M_2^2 = \frac{36M_\infty^4 \sin^2\theta - 5\left(M_\infty^2 \sin^2\theta - 1\right)\left(7M_\infty^2 \sin^2\theta + 5\right)}{\left(7M_\infty^2 \sin^2\theta - 1\right)\left(M_\infty^2 \sin^2\theta + 5\right)} \tag{2}$$

From normal-shock relationships,

$$\frac{p_{t,3}}{p_{t,2}} = \left(\frac{6M_2^2}{M_2^2 + 5}\right)^{7/2} \left(\frac{6}{7M_2^2 - 1}\right)^{5/2} \tag{3}$$

From one-dimensional isentropic flow relationships,

$$\frac{p_2}{p_{t,2}} = \left(1 + \frac{M_2{}^2}{5}\right)^{-7/2} \tag{4}$$

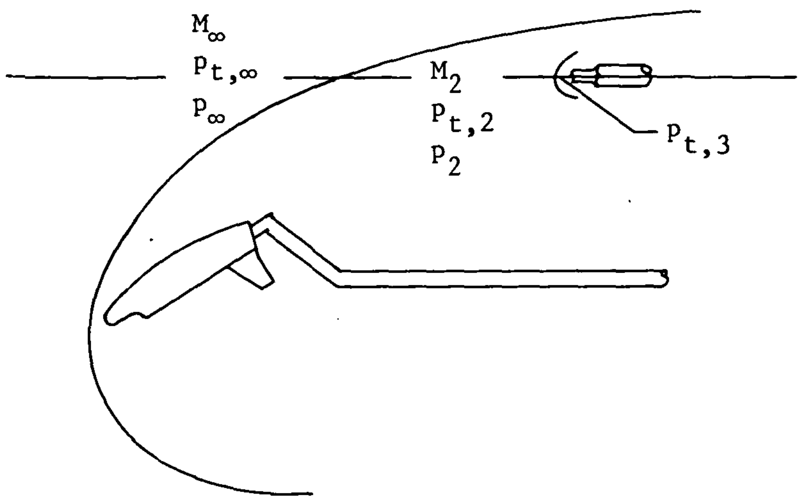

A shock angle (θ) was assumed, and initial values for $p_{t,2}$ and M_2 were computed from equations (1) and (2). The computed value of M_2 and the measured pitot pressure ($p_{t,3}$) were used in equation (3) to determine another value for $p_{t,2}$. The series of calculations was repeated with different shock angles (θ) until the two values of $p_{t,2}$ converged. After convergence was obtained, equation (4) was used to calculate p_2.

This type of calculation, wherein $p_{t,3}$ is the only known quantity behind the shock, is valid only near the shock. As the probe moves aft from the bow shock, M_2 is not constant along the path from the shock to the probe and this method does not give a unique solution for M_2, $p_{t,2}$, and p_2. The accuracy of the static pressure decreases directly with distance behind the shock. Nonetheless, the correct value of p_2 at the shock establishes the peak overpressure, and the remainder of the values computed from the pitot pressure along with the values from the static-pressure probe are useful for establishing the signature curves.

RESULTS AND DISCUSSION

The measured pressures at several meridional angles are presented in table I for the launch configuration at an angle of attack of 0° and in table II for the orbiter at four angles of attack. For the launch configuration, the pressure probes were located at $h/l = 10.65$, and for the orbiter, they were located at $h/l = 1.176$. Pressure signatures for the launch configuration at two meridional angles and for the orbiter at several angles of attack are presented in figures 4 and 5, respectively. Although the meridional angles for the static-pressure and pitot-pressure probe surveys of the equivalent body of revolution differed by 8.5°, the two sets of values were used as if they were along the same meridian. The pressure signatures are plotted relative to an arbitrary origin.

There is a large difference between the values of static pressure from the two probes near the shock in both figures 4 and 5. The value from the static probe is extremely high relative to that from the pitot probe, an indication of a strong interference effect of the shock. Previous comparisions of measurements from the two probes (not presented) showed that the static probe can only be used to measure static pressure near weak waves ($\Delta p/p_\infty \leqq 0.5$). Reference 12 also provides data demonstrating the inadequacy of simple static-pressure probes in the vicinity of a strong shock.

As previously discussed, the static pressures obtained from the pitot-pressure measurements are only accurate at the shock and become progressively less accurate with distance behind the shock. In contrast, the pressures measured with the static probe become more accurate when the probe tip clears the shock in its rearward movement; its primary source of error, once it is free of the shock, is flow angularity. The pressure signatures were faired between the two sets of data by using the pitot-probe value at the shock, favoring the pitot-probe values near the shock, and favoring the static-probe values after the probe has completely cleared the shock.

Estimations of the pressure signatures using the computer codes of references 13 and 14 are also superimposed on the appropriate plots in figures 4 and 5. The geometric shape for the configuration used in the computer programs is shown in the key of each figure. The cylindrical extension behind the plume for the configuration of figure 4 was necessary, because of flow overexpansion, for the program to continue to calculate the flow field far enough beyond the trailing edge of the plume to position the shock at the required h/l from the reference axis. The cylinder has no effect on the shock shape in the region of interest (see ref. 15). The orbiter presented a similar problem. The computer program would not run far enough downstream for the shock to be at the required h/l and could not compute the flow field for angles of attack greater than 25°. Since only the flow field of the windward surface is of interest, the upper surface can be judiciously contoured to make the program run for an angle of attack of 30°, but only for a small distance beyond the length of the configuration. To make the program run the required distance for the shock to be at the desired h/l, an established experimental observation was utilized. It has been shown (e.g., see refs. 16 and 17) that, for a delta wing configuration at angles of attack above 20°, a body of revolution generated by the lower surface contour in the plane of symmetry has, at an angle of attack of 0°, approximately the same flow field as the delta wing configuration does in that plane. Therefore, such an equivalent body of revolution was used in the program to calculate the flow field for an angle of attack of 30°. The results are shown in figure 5(c), and the calculated and measured pressure signatures agree very well. Calculations using a body of revolution for the configuration at an angle of attack of 20° (not presented) confirmed the inadequacy of the principle at the lower angles of attack. Also, the program would not operate at $\alpha = 40^\circ$ because subsonic Mach numbers in the axial direction occur near the nose. The calculated locations of the bow shock from the orbiter were slightly different from the measured locations, but because the peak overpressure and the impulse (function of area under the curve) are the most important parameters, the calculated and measured results were plotted as if the shocks were at the same location.

A comparison of the calculated values and measured pitot-probe values for the launch configuration (fig. 4) shows excellent agreement between peak values of pressure and very good agreement between the overall signatures. For the orbiter at $\alpha = 30^{\circ}$ (fig. 5(c)), the calculated peak values are lower than the measured pitot-probe values, but the areas under the signatures are about the same. For these conditions the excellent predictions of signature areas and peak overpressures show that theoretical estimates are acceptable as initial conditions for extrapolation to ground level to establish the intensity of the resulting sonic boom.

Since the angle of attack for the orbiter at Mach 6 is 25° as it descends from orbit, a carpet plot of the faired pressure signatures is presented in figure 6(a) from which the interpolated pressure signature for $\alpha = 25^{\circ}$ (fig. 6(b)) was obtained. The calculated pressure signature is included in figure 6(b) for comparison and shows that, although the peak overpressure is underpredicted, the areas under the signatures are in good agreement.

A carpet plot of the peak overpressures from the pitot-probe measurements is provided in figure 7 for the complete set of angles of attack and meridional angles. When viewed in this total perspective, it is clear that the peak overpressure directed towards the ground is reduced for ray (meridional) angles greater than 0°. The linear variation of the peak overpressure with angle of attack for $\theta = 0^{\circ}$ does not hold at all meridional angles.

CONCLUDING REMARKS

Static-pressure signatures parallel to the flight path of the launch and entry configurations of the space shuttle have been measured in the Langley 20-inch Mach 6 tunnel in air at selected distances from the flight path. The launch configuration, consisting of an equivalent body of revolution (representing the orbiter and external fuel tank) with a solid exhaust gas plume attached, was tested at an angle of attack of 0°. The entry configuration (orbiter alone) was tested over an angle-of-attack range from 10° to 40°.

Results from the tests show that conventional static-pressure probes cannot be used in the vicinity of a strong shock but can be used when completely behind the shock; a pitot probe gives more accurate values at the shock. This observation is reinforced by the agreement between the peak overpressure calculated from a finite-difference method and the value obtained from the pitot-pressure measurement.

The areas under the calculated pressure signatures were found to be in good agreement with those under the measured signatures for the launch configuration and the entry configuration at angles of attack of 25° and 30°. These excellent predictions of signature areas and peak overpressures show that theoretical estimates are acceptable as initial conditions for extrapolation to ground level to establish the intensity of the resulting sonic boom. Wind-tunnel measurements would be needed on a limited basis to verify the results.

Langley Research Center
National Aeronautics and Space Administration
Hampton, VA 23665
February 23, 1979

REFERENCES

1. Holloway, Paul F.; Wilhold, Gilbert A.; Jones, Jess H.; Garcia, Frank, Jr.; and Hicks, Raymond M.: Shuttle Sonic Boom - Technology and Predictions. AIAA Paper No. 73-1039, Oct. 1973.

2. Hicks, Raymond M.; Mendoza, Joel P.; and Thomas, Charles L.: Pressure Signatures for the Apollo Command Module and the Saturn V Launch Vehicle With a Discussion of Strong Shock Extrapolation Procedures. NASA TM X-62117, 1972.

3. Hicks, Raymond M.; Mendoza, Joel P.; and Garcia, Frank, Jr.: A Wind-Tunnel Flight Correlation of Apollo 15 Sonic Boom. NASA TM X-62111, 1972.

4. Carlson, Harry W.: Simplified Sonic-Boom Prediction. NASA TP-1122, 1978.

5. Carlson, Harry W.; and Mack, Robert J.: A Wind-Tunnel Study of the Applicability of Far-Field Sonic-Boom Theory to the Space Shuttle Orbiter. NASA TP-1186, 1978.

6. Garcia, Frank, Jr.; Hicks, Raymond M.; and Mendoza, Joel P.: A Wind Tunnel Flight Correlation of Apollo 16 Sonic Boom. NASA TM X-62073, 1973.

7. Hicks, Raymond M.; and Mendoza, Joel P.: An Investigation of the Feasibility of Simulating Gaseous Exhaust Plumes With Solid Bodies in Sonic Boom Studies. NASA TM X-62131, 1973.

8. Mendoza, Joel P.: Sonic Boom Pressure Signatures for the Space Shuttle Launch Vehicle. NASA TM X-62441, 1975.

9. Mendoza, Joel P.: Further Wind Tunnel Measurements of Pressure Signatures for a 0.0041-Scale Model of the Space Shuttle Orbiter. NASA TM X-73120, 1976.

10. Goldberg, Theodore J.; and Hefner, Jerry N. (appendix by James C. Emery): Starting Phenomena for Hypersonic Inlets With Thick Turbulent Boundary Layers at Mach 6. NASA TN D-6280, 1971.

11. Ames Research Staff: Equations, Tables, and Charts for Compressible Flow. NACA Rep. 1135, 1953. (Supersedes NACA TN 1428.)

12. Carlson, Harry W.; and Mack, Robert J.: A Study of the Sonic-Boom Characteristics of a Blunt Body at a Mach Number of 4.14. NASA TP-1015, 1977.

13. Marconi, Frank; Salas, Manuel; and Yaeger, Larry: Development of a Computer Code for Calculating the Steady Super/Hypersonic Inviscid Flow Around Real Configurations. Volume I - Computational Technique. NASA CR-2675, 1976.

14. Marconi, Frank; and Yaeger, Larry: Development of a Computer Code for Calculating the Steady Super/Hypersonic Inviscid Flow Around Real Configurations. Volume II - Code Description. NASA CR-2676, 1976.

15. Inouye, Mamoru; and Lomax, Harvard: Comparison of Experimental and Numerical Results for the Flow of a Perfect Gas About Blunt-Nosed Bodies. NASA TN D-1426, 1962.

16. Keyes, J. Wayne; and Ashby, George C., Jr.: Calculated and Experimental Hinge Moments on a Trailing-Edge Flap of a 75° Swept Delta Wing at Mach 6. NASA TN D-4268, 1967.

17. Ashby, George C., Jr.; and Helms, Vernon T., III: Flow-Field Surveys on the Windward Side of the NASA 040A Space Shuttle Orbiter at 31° Angle of Attack and Mach 20 in Helium. NASA TM X-3560, 1977.

TABLE I.- MEASURED NEAR-FIELD STATIC PRESSURES FOR SPACE SHUTTLE LAUNCH CONFIGURATION

(a) Static-pressure probe

[h/l = 10.65]

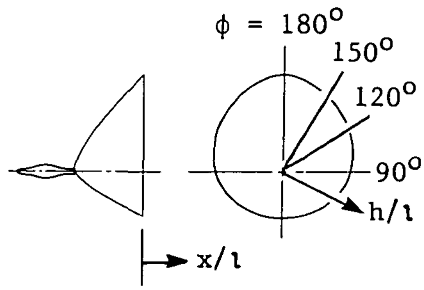

φ = 68.5°		φ = 98.5°		φ = 128.2°		φ = 158.2°	
x/l	$\Delta p/p_\infty$	x/l	$\Delta p/p_\infty$	x/l	$\Delta p/p_\infty$	x/l	$\Delta p/p_\infty$
20.443	0.0928	19.983	0.0605	17.036	0.0138	16.167	0.0085
22.147	.0877	20.443	.0572	17.871	.0811	17.411	.7559
23.850	.0831	21.312	1.1500	18.382	.0065	17.411	1.2160
24.736	.0722	21.567	2.3430	18.893	.4868	17.683	2.9340
25.486	.4729	22.555	1.5540	19.046	1.8130	17.717	3.2740
25.843	1.6580	23.867	1.1380	19.267	2.8910	17.939	3.0890
26.065	1.7330	27.257	.6536	19.557	2.6070	18.995	1.7520
26.133	1.7080	30.681	.3498	19.659	2.4230	20.443	1.2450
26.235	1.6540	33.203	.1902	20.426	1.6420	22.164	.9003
26.422	1.5050	35.758	.0853	22.129	1.1130	25.554	.4422
27.274	1.1500	33.203	.1960	23.816	.8192	28.961	.1695
28.927	.8715	30.698	.3535	27.257	.4015	31.516	.0310
32.368	.5240	27.308	.6561	30.681	.1493	34.072	-.0674
35.775	.2870	23.850	1.1660	33.169	.0251	31.482	.0307
38.330	.1624	22.164	1.9050	35.758	-.0670	28.995	.1689
40.886	.0684	21.430	1.5970	33.220	.0236	25.571	.4419
38.348	.1614	20.426	.0499	30.716	.1500	22.164	.9007
35.775	.2878	20.153	.0502	27.257	.4047	20.562	1.2200
32.385	.5217	18.739	.0517	23.850	.8176	19.557	1.5120
28.944	.8662	17.019	.0542	22.249	1.0890	18.739	1.9650
27.257	1.1500			20.494	1.6230	17.666	1.8600
25.554	.7323			19.625	2.5220	17.104	-.0219
24.702	.0553			18.266	-.0220	15.332	-.0243
22.998	.0546			17.836	-.0218		
20.427	.0596			17.019	-.0214		

TABLE I.- Concluded

(b) Pitot-pressure probe

[h/l = 10.65]

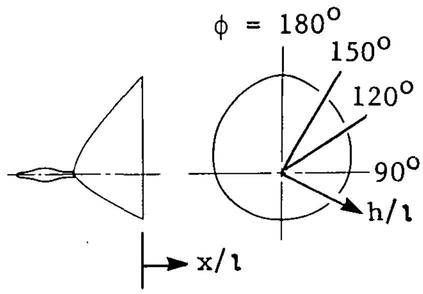

φ = 90°		φ = 120°		φ = 150°		φ = 180°	
x/l	$\Delta p/p_\infty$	x/l	$\Delta p/p_\infty$	x/l	$\Delta p/p_\infty$	x/l	$\Delta p/p_\infty$
20.443	0.0938	17.853	0.0664	17.036	0.0490	16.167	0.0371
22.147	.0856	18.739	.0597	17.871	.0413	17.411	.8756
22.998	.0790	19.591	.4494	18.382	1.6540	17.411	1.0360
23.714	1.3750	19.847	1.5710	18.893	1.4760	17.683	1.6500
23.850	1.3760	19.881	1.5590	19.046	1.4100	17.717	1.6240
23.867	1.3360	19.983	1.5230	19.267	1.3440	17.939	1.5650
24.259	1.2630	20.443	1.3940	19.557	1.2800	18.995	1.2420
24.736	1.1620	21.312	1.1860	19.659	1.2420	20.443	.9249
25.486	1.0380	21.567	1.1300	20.426	1.0680	22.164	.6469
25.537	1.0160	22.555	.9443	22.129	.7634	25.554	.2685
26.065	.9359	23.867	.7387	23.816	.5363	28.961	.0575
26.422	.8781	27.257	.3659	27.257	.2141	31.516	-.0466
27.274	.7729	30.681	.1402	30.681	.0235	34.072	-.1262
28.927	.5871	33.203	.0265	33.169	-.0754	31.482	-.0468
32.368	.3053	35.758	-.0572	35.758	-.1456	28.995	.0596
35.775	.1263	33.203	.0299	33.220	-.0759	25.571	.2748
38.330	.0280	30.698	.1439	30.716	.0250	22.164	.6475
40.886	-.0440	27.308	.3706	27.257	.2194	20.562	.9031
38.348	.0294	23.850	.7575	23.850	.5392	19.557	1.1010
35.775	.1295	22.164	1.0160	22.249	.7400	18.739	1.2990
32.385	.3060	21.430	1.1650	20.494	1.0450	17.666	1.6490
28.944	.5829	20.426	1.4000	19.625	1.2380	17.104	.0124
27.257	.7709	20.153	1.4800	18.266	1.5770	15.332	.0271
25.554	1.0120	19.847	1.4810	17.836	.0257		
24.702	1.1640	18.739	.0545	17.019	.0333		
23.867	1.3390	17.019	.0654				
23.816	1.3690						
22.998	.0711						
20.427	.0903						

TABLE II.- MEASURED NEAR-FIELD STATIC PRESSURES FOR SPACE SHUTTLE ORBITER

(a) $\alpha = 10^{\circ}$; static-pressure probe

$[h/l = 1.176]$

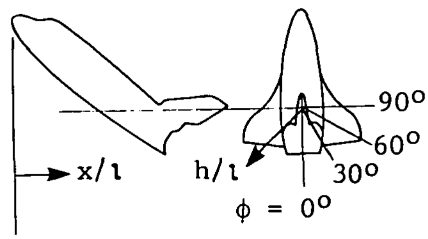

$\phi = 0^{\circ}$		$\phi = 21.5^{\circ}$		$\phi = 30^{\circ}$		$\phi = 60^{\circ}$		$\phi = 90^{\circ}$	
x/l	$\Delta p/p_{\infty}$	x/l	$\Delta p/p_{\infty}$	x/l	$\Delta p/p_{\infty}$	x/l	$\Delta p/p_{\infty}$	x/l	$\Delta p/p_{\infty}$
3.9526	0.0955	3.9996	0.0152	3.9526	0.0400	3.9469	0.0282	4.1389	0.0325
4.0467	.0906	4.0191	.3316	4.1427	.8074	4.1013	.2330	4.2688	.0295
4.1351	.1235	4.1389	.9288	4.2161	.6879	4.1163	.3196	4.2801	.0262
4.1408	.2568	4.1709	.9452	4.2198	.6659	4.1182	.3446	4.3234	.0262
4.1464	.3578	4.1784	.9156	4.2292	.6555	4.1257	.3816	4.4043	.0259
4.1558	.5968	4.1822	.9123	4.2311	.6612	4.1464	.4430	4.4984	.3827
4.1671	.7584	4.1911	.8922	4.2481	.6356	4.1556	.4823	4.5379	.4865
4.1803	1.0434	4.1954	.8774	4.2876	.5995	4.1765	.4935	4.5586	.4918
4.1822	1.1542	4.2368	.7695	4.3328	.5606	4.1897	.4852	4.5887	.4805
4.1973	1.3924	4.3309	.6226	4.4250	.4964	4.2443	.4478	4.6076	.4676
4.2349	1.3492	4.5153	.5280	4.5135	.4421	4.3290	.3672	4.7092	.3830
4.3290	1.0465	5.0386	.3262	4.7073	.3465	4.5135	.3300	5.0762	.2330
4.4306	.8820	5.2701	.1320	4.8937	.2683	4.8937	.1881	5.4545	.0995
4.5191	.7696	5.6446	-.0126	5.2682	.1670	5.1026	.1617	5.8347	.0113
4.6132	.6799	5.9307	-.0787	5.6446	.0539	5.2795	.1090	5.9037	-.0067
4.7073	.5984	6.2112	-.1347	5.8366	.0040	5.7444	.0092	5.4621	.0940
4.9012	.4597	5.9307	-.0769	6.1811	-.0772	5.4621	.0626	5.0800	.2260
5.0819	.3489	5.6465	-.0091	5.8385	.0024	4.8918	.1863	4.7186	.3671
5.2720	.2487	5.2701	.1374	5.6503	.0513	4.5172	.3193	4.3968	.0038
5.4602	.1615	4.8937	.3293	5.2701	.1621	4.1069	.1449	4.3045	.0023
5.6484	.0859	4.5172	.5159	4.8880	.2580	4.0937	.0371	4.1521	.0043
5.8347	.0220	4.3234	.6322	4.5116	.4243	3.9469	-.0019	3.7644	.0141
6.0248	-.0309	4.1897	.8872	4.3328	.5412	3.5761	.0065		
6.1284	-.0576	4.1370	.8343	4.2405	.6205				
5.8479	.0168	3.9488	-.0270	4.1991	.6872				
5.6541	.0813			4.1408	.7549				
5.2757	.2442			3.9507	-.0032				
4.8993	.4562								
3.9526	.0528								

TABLE II.- Continued

(b) $\alpha = 10^{\circ}$; pitot-pressure probe

$[h/l = 1.176]$

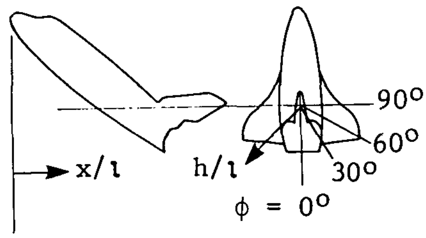

$\phi = 0^{\circ}$		$\phi = 8.5^{\circ}$		$\phi = 21.5^{\circ}$		$\phi = 38.5^{\circ}$		$\phi = 68.5^{\circ}$	
x/l	$\Delta p/p_{\infty}$	x/l	$\Delta p/p_{\infty}$	x/l	$\Delta p/p_{\infty}$	x/l	$\Delta p/p_{\infty}$	x/l	$\Delta p/p_{\infty}$
3.9996	0.0510	3.9526	0.0557	3.9526	0.0815	3.9469	0.0238	4.1389	0.0347
4.0919	.0432	4.1427	.0471	4.0467	.0740	4.1013	.4398	4.2688	.3034
4.1389	.0491	4.2161	.4572	4.1351	.2747	4.1163	.6028	4.2801	.3769
4.1709	.6148	4.2198	.7959	4.1408	.6185	4.1182	.6007	4.3234	.3543
4.1784	.9991	4.2292	1.0159	4.1464	.7430	4.1257	.5916	4.4043	.3536
4.1822	1.0254	4.2311	1.0092	4.1521	.7606	4.1464	.5762	4.4984	.3160
4.1954	1.0134	4.2481	.9835	4.1558	.7531	4.1556	.5698	4.5379	.3007
4.1973	1.0176	4.2876	.9294	4.1671	.7440	4.1765	.5582	4.5586	.2952
4.2368	.9598	4.3328	.8717	4.1803	.7322	4.1897	.5462	4.5887	.2813
4.3309	.8300	4.4250	.7615	4.1973	.7113	4.2443	.5107	4.6076	.2751
4.5153	.6295	4.5135	.6690	4.2349	.6723	4.3290	.4509	4.7092	.2931
5.0386	.3395	4.7073	.5034	4.3290	.5946	4.5135	.3318	5.0762	.1554
5.2701	.1188	4.8937	.3582	4.4306	.5205	4.8937	.1627	5.4545	.0451
5.6446	-.0174	5.2682	.1497	4.5191	.4674	5.1026	.1219	5.8347	-.0417
5.9307	-.0943	5.6446	-.0052	4.6132	.4110	5.2795	.0618	5.9307	-.0595
6.2112	-.1547	5.8366	-.0753	4.7073	.3651	5.7444	-.0166	5.4621	.0450
5.9307	-.0940	6.1811	-.1670	4.9012	.3414	5.4621	.0061	5.0800	.1560
5.6465	-.0111	5.8385	-.0773	5.0819	.2483	4.8918	.1690	4.7186	.2833
5.2701	.1262	5.6503	-.0038	5.2720	.1623	4.5172	.3315	4.3968	.3357
4.8937	.3406	5.2701	.1511	5.4602	.0891	4.1069	.3045	4.3045	.3503
4.5172	.6306	4.8880	.3599	5.6484	.0165	4.0937	.0749	4.1521	.0183
4.3234	.8401	4.5116	.6556	5.8347	-.0351	3.9461	.0094	3.7644	.0331
4.1897	1.0172	4.3328	.8475	6.0248	-.0855	3.5761	.0251		
4.1370	.0248	4.2405	.9600	6.1284	-.1059				
3.9488	.0397	4.2010	.0192	5.8470	-.0405				
		4.1991	.0185	5.6541	.0119				
		4.1860	.0145	5.2757	.1660				
		4.1408	.0204	4.8993	.3430				
		3.9507	.0212	4.5135	.4663				

TABLE II.- Continued

(c) $\alpha = 20^{\circ}$; static-pressure probe

$[h/l = 1.176]$

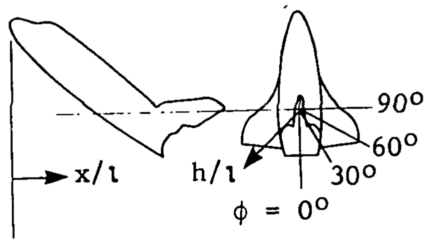

$\phi = 0^{\circ}$		$\phi = 21.5^{\circ}$		$\phi = 30^{\circ}$		$\phi = 60^{\circ}$		$\phi = 90^{\circ}$	
x/l	$\Delta p/p_{\infty}$	x/l	$\Delta p/p_{\infty}$	x/l	$\Delta p/p_{\infty}$	x/l	$\Delta p/p_{\infty}$	x/l	$\Delta p/p_{\infty}$
2.9115	0.0641	3.0152	0.0789	3.0040	0.0513	3.0115	0.0732	3.3898	0.0346
3.0792	.6945	3.0830	.5073	3.1018	.1026	3.1094	.0729	3.4858	.0332
3.1056	3.7118	3.1169	2.5952	3.1075	.1518	3.1865	.0685	3.5950	.0218
3.1150	4.3136	3.1414	3.2154	3.1169	.4211	3.2035	.0685	3.9582	.0171
3.1206	4.2251	3.1526	3.0034	3.1301	.6541	3.2373	.0660	4.0504	.2906
3.1809	3.0104	3.1997	2.5249	3.1414	1.2053	3.3051	.2351	4.0956	.7346
3.1865	2.9557	3.2053	2.4589	3.1451	1.4427	3.3634	1.1308	4.1427	.7598
3.1978	2.8313	3.2976	1.8263	3.1715	2.4519	3.3917	1.1029	4.1954	.6937
3.2053	2.6932	3.3898	1.5052	3.2016	2.1872	3.5743	.7741	4.2349	.6434
3.2411	2.4322	3.5761	1.1029	3.2957	1.5909	3.7662	.5891	4.3271	.5634
3.3013	2.0679	3.7662	.8078	3.3879	1.3067	3.9582	.5041	4.5191	.4363
3.4049	1.6432	4.1389	.4285	3.5799	1.0655	4.3328	.3086	4.7205	.3137
3.4820	1.4261	4.5153	.1757	3.7662	.8220	4.7036	.1899	5.0762	.1612
3.5780	1.2240	4.7995	.0416	4.1427	.4553	4.9953	.1421	5.2776	.0920
3.7587	.8734	5.0800	-.0598	4.5172	.2063	5.2682	.0679	5.4583	.0405
3.9563	.6431	4.7977	.0439	4.7577	.0729	5.0819	.1234	5.2757	.0925
4.1427	.4626	4.5191	.1778	5.0838	-.0144	4.9953	.1396	5.0819	.1578
4.5078	.1891	4.1408	.4413	4.7995	.0718	4.7073	.1873	4.9068	.2229
4.8955	-.0069	3.7662	.8242	4.5229	.2037	4.3234	.3080	4.5191	.4292
5.0800	-.0736	3.5743	1.1235	4.1464	.4548	3.9488	.5016	4.1427	.7456
4.8993	-.0090	3.3954	1.5192	3.7662	.8193	3.7644	.5846	3.7662	-.0085
4.5247	.1780	3.2882	1.9336	3.6495	.9750	3.5253	.8229	3.5700	-.0070
4.1351	.4660	3.0924	.2185	3.4858	1.1110	3.3315	.4949	3.3879	-.0027
3.7662	.8555	3.0152	.0442	3.3954	1.2862	3.1922	.0334	3.1997	.0027
3.3898	1.6832			3.2900	1.6310	3.0096	.0373		
3.1959	2.8348			3.1997	2.2699				
2.8214	.0280			3.1112	.0725				
				3.0058	.0234				
				2.8233	.0266				

TABLE II.- Continued

(d) $\alpha = 20^{\circ}$; pitot-pressure probe

$[h/l = 1.176]$

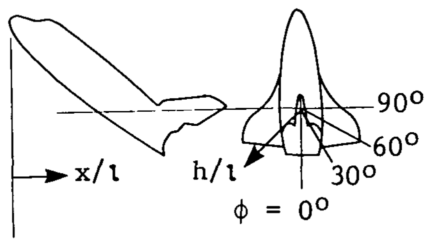

$\phi = 0^{\circ}$		$\phi = 8.5^{\circ}$		$\phi = 21.5^{\circ}$		$\phi = 38.5^{\circ}$		$\phi = 68.5^{\circ}$	
x/l	$\Delta p/p_{\infty}$	x/l	$\Delta p/p_{\infty}$	x/l	$\Delta p/p_{\infty}$	x/l	$\Delta p/p_{\infty}$	x/l	$\Delta p/p_{\infty}$
3.0152	0.0437	3.0040	0.0256	2.9155	0.0489	3.0115	0.0742	3.3898	0.0287
3.0830	2.1384	3.1018	.3815	3.0096	.0413	3.1094	.0641	3.4858	.0198
3.1169	1.9935	3.1075	.6918	3.0792	.0353	3.1865	.4934	3.5686	.4081
3.1206	2.0162	3.1169	2.0422	3.1056	.0333	3.1978	1.3138	3.5799	.6792
3.1414	1.9387	3.1244	2.0349	3.1150	.0320	3.2035	1.3043	3.5912	.6665
3.1526	1.8495	3.1301	2.0261	3.1206	.0307	3.2148	1.2836	3.5950	.6706
3.1997	1.6798	3.1414	1.9745	3.1809	.1604	3.2373	1.2418	3.6721	.6009
3.2053	1.6597	3.1451	1.9494	3.1865	.3475	3.3051	1.1159	3.7738	.5174
3.2976	1.3828	3.1715	1.8461	3.1978	.8813	3.3634	1.0323	3.8867	.4475
3.3898	1.1532	3.2016	1.7411	3.2035	1.2770	3.3917	.9866	3.9582	.4304
3.5761	.7999	3.2957	1.4487	3.2053	1.5553	3.5743	.7642	4.0504	.3673
3.7662	.5322	3.3879	1.2110	3.2110	1.5709	3.7662	.5682	4.0956	.3391
4.1389	.1636	3.5799	.8340	3.2411	1.4726	3.9582	.4009	4.1427	.3153
4.5153	-.0504	3.7662	.5663	3.3013	1.3331	4.3328	.2234	4.1954	.2882
4.7995	-.1587	4.1427	.1964	3.4049	1.2054	4.7036	.0574	4.2349	.2707
5.0800	-.2375	4.5172	-.0251	3.4820	1.0708	4.9953	-.0372	4.3271	.2330
4.7977	-.1531	4.7577	-.1477	3.5780	.9162	5.2682	-.1082	4.5191	.1570
4.5191	-.0477	5.0838	-.2370	3.7587	.6561	5.0819	-.0589	4.7205	.1607
4.1408	.1740	4.7995	-.1435	3.9563	.4490	4.9953	-.0387	5.0762	.0716
3.7662	.5484	4.5229	-.0234	4.1427	.2994	4.7073	.0591	5.2776	.0130
3.5743	.8105	4.1464	.2043	4.5078	.0804	4.3234	.2325	5.4583	-.0391
3.3954	1.1457	3.7662	.5737	4.8955	-.0872	3.9488	.4077	5.2757	.0135
3.2882	1.4109	3.6495	.7330	5.0800	-.1451	3.7644	.5740	5.0819	.0701
3.0924	2.1158	3.4858	1.0074	4.8993	-.0873	3.5253	.8159	4.9068	.1013
3.0152	.0234	3.3954	1.1955	4.5247	.0763	3.3315	1.0600	4.5191	.1538
		3.2900	1.4605	4.1351	.3102	3.1922	.8595	4.1427	.3097
		3.1997	1.7339	3.7662	.6499	3.0115	.0431	3.7662	.5103
		3.0058	.0167	3.3898	1.2149			3.5761	.2448
		2.8233	.0248	2.8214	.0258			3.1997	.0139

TABLE II.- Continued

(e) $\alpha = 30^\circ$; static-pressure probe

$[h/l = 1.176]$

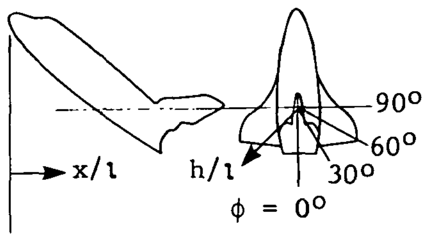

$\phi = 0^\circ$		$\phi = 21.5^\circ$		$\phi = 30^\circ$		$\phi = 60^\circ$		$\phi = 90^\circ$	
x/l	$\Delta p/p_\infty$	x/l	$\Delta p/p_\infty$	x/l	$\Delta p/p_\infty$	x/l	$\Delta p/p_\infty$	x/l	$\Delta p/p_\infty$
2.0704	0.0307	2.2567	0.0483	2.0742	0.0835	2.4017	0.0940	2.8214	0.0712
2.2586	.0325	2.3301	3.6115	2.2586	.0726	2.4995	.0868	2.9174	.0647
2.3433	8.7547	2.3452	8.2823	2.3226	.0791	2.5052	.0822	2.9474	.0599
2.3527	9.6752	2.3621	8.4351	2.3301	.1019	2.5202	.0848	2.9625	.0562
2.3734	8.7973	2.3640	8.2280	2.3358	.1389	2.6407	.0801	2.9738	.0546
2.3941	7.6625	2.4468	5.2459	2.3564	.2845	2.7047	1.2329	2.9757	.0491
2.4129	6.8706	2.6313	2.6241	2.3904	1.3098	2.7179	2.1077	2.9832	.0514
2.4337	6.1757	3.0096	1.1178	2.4393	6.5535	2.7593	2.0928	3.0077	.0534
2.4412	5.9139	3.3879	.5250	2.5391	4.0180	2.7894	1.8887	3.0134	.0463
2.4562	5.5252	3.6684	.2520	2.6369	2.7479	2.8233	1.6544	3.1056	.0441
2.4600	5.3567	3.9526	.0671	2.8233	1.7258	3.1978	.8554	3.2035	.0411
2.4882	4.7951	3.6702	.2519	3.2016	.8359	3.5837	.5676	3.2976	.0348
2.4995	4.6567	3.3917	.5211	3.5780	.4065	3.9507	.3062	3.3879	.0257
2.5278	4.2132	3.0096	1.1027	3.8566	.1992	4.2311	.1980	3.4839	.4438
2.6332	2.9566	2.6426	2.9145	4.1389	.0479	4.5210	.1619	3.5423	1.3847
2.8252	1.7790	2.4449	5.4175	3.8660	.1917	4.2405	.1939	3.5780	1.2641
3.0077	1.1889	2.3621	8.5957	3.5837	.3991	3.9546	.3038	3.6702	1.0083
3.3898	.5481	2.2624	.0072	3.1997	.8240	3.5761	.5714	3.7644	.8622
3.6684	.2576	2.0742	-.0032	2.8251	1.7180	3.1997	.8449	4.1427	.5180
3.9507	.0513			2.6332	2.7818	3.0924	.9818	4.5153	.2842
3.6665	.2551			2.3339	.0899	3.0096	1.1107	4.7977	.1574
3.3898	.5448			2.0723	.0542	2.5334	.0517	5.0800	.0799
2.6482	2.9033					2.2586	.0543	4.8014	.1550
2.4468	5.8975							4.5153	.2825
2.2530	.0087							4.1389	.5191
1.8784	.0111							3.7681	.8523
								3.5780	1.2674
								3.4557	.0129
								2.9964	.0151

TABLE II.- Continued

(f) $\alpha = 30^{\circ}$; pitot-pressure probe

$[h/l = 1.176]$

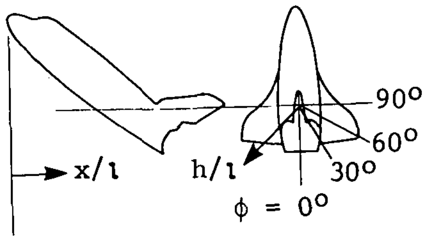

φ = 0°		φ = 8.5°		φ = 21.5°		φ = 38.5°		φ = 68.5°	
x/l	$\Delta p/p_{\infty}$	x/l	$\Delta p/p_{\infty}$	x/l	$\Delta p/p_{\infty}$	x/l	$\Delta p/p_{\infty}$	x/l	$\Delta p/p_{\infty}$
2.2567	0.0005	2.0742	0.0385	2.0704	0.0102	2.4017	0.0647	2.8214	0.0566
2.3301	-.0067	2.2586	.0266	2.1683	.0063	2.4995	.5282	2.9174	.0468
2.3452	1.5858	2.3226	2.5528	2.2586	.0074	2.5052	2.0179	2.9475	.2839
2.3621	3.3440	2.3301	3.6238	2.3433	.0016	2.5127	2.2878	2.9625	.7210
2.3640	3.2680	2.3358	3.5364	2.3527	.0022	2.5202	2.2926	2.9738	1.1241
2.4468	2.4449	2.3565	3.3164	2.3734	-.0012	2.5315	2.2245	2.9757	1.1410
2.6312	1.4159	2.3904	2.9817	2.3941	-.0033	2.6407	1.7626	2.9832	1.1198
3.0096	.4230	2.4393	2.5215	2.4129	-.0030	2.7047	1.5721	3.0077	1.0806
3.3879	-.0414	2.5391	1.8805	2.4338	.3588	2.7179	1.5317	3.0134	1.0062
3.6684	-.2233	2.6369	1.4213	2.4374	1.2415	2.7593	1.3854	3.1056	.9063
3.9526	-.3399	2.8233	.8111	2.4412	1.3549	2.7894	1.3154	3.2035	.7645
3.6702	-.2184	3.2016	.1673	2.4487	2.8978	2.8233	1.2217	3.2976	.6876
3.3917	-.0344	3.5780	-.1524	2.4562	2.8723	3.1978	.5469	3.3879	.6258
3.0096	.4318	3.8566	-.2927	2.4600	2.8041	3.5837	.1276	3.4839	.5299
2.6426	1.3794	4.1389	-.3920	2.4882	2.5861	3.9507	-.0675	3.5423	.4733
2.4449	2.4587	3.8660	-.2967	2.4995	2.5233	4.2311	-.1690	3.5780	.4408
2.3621	3.1694	3.5837	-.1523	1.7356	2.6332	4.5210	-.2397	3.6702	.3708
2.2624	-.0270	3.1997	.1757	2.8252	1.0401	4.2405	-.1697	3.7644	.3135
2.0742	-.0259	2.8251	.8089	3.0077	.6364	3.9545	-.0664	4.1427	.2689
		2.6332	1.4214	3.3898	.1506	3.5761	.1340	4.5153	.0757
		2.3390	3.5079	3.6684	-.0526	3.1997	.5427	4.7977	-.0145
		2.0723	.0308	3.9507	-.1935	3.0924	.7187	5.0800	-.0764
				3.6665	-.0478	3.0096	.8824	4.8014	-.0148
				3.3898	.1625	2.5334	2.1354	4.5153	.0781
				2.6482	1.6930	2.2586	.0645	4.1389	.2722
				2.4468	.5716			3.5780	.4334
				2.2530	-.0063			3.3879	.6038
				1.8784	.0128			2.9964	1.0596
								2.8214	.0284

TABLE II.- Continued

(g) α = 40°; static-pressure probe

[h/l = 1.176]

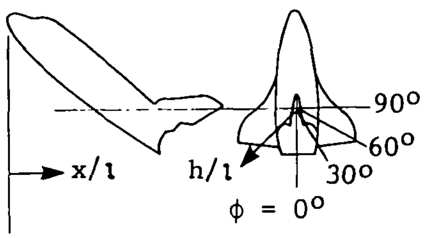

ϕ = 0°		ϕ = 21.5°		ϕ = 30°		ϕ = 60°		ϕ = 90°	
x/l	$\Delta p/p_\infty$	x/l	$\Delta p/p_\infty$	x/l	$\Delta p/p_\infty$	x/l	$\Delta p/p_\infty$	x/l	$\Delta p/p_\infty$
1.8521	0.3183	1.6958	0.0461	1.6921	0.0596	2.0647	0.0433	2.4412	0.0361
1.9085	12.2957	1.8784	.2605	1.9104	.5163	2.1400	.0419	2.5409	.0340
2.0083	8.4669	1.9198	10.5728	1.9349	2.3555	2.1551	.0405	2.6369	.0297
2.0120	8.3731	1.9349	11.9087	1.9386	6.7885	2.1701	.0420	2.8120	.6180
2.0723	6.4448	1.9386	13.2160	2.0704	6.7241	2.2454	.2974	2.8609	2.2085
2.2548	3.2652	1.9725	10.6418	2.2605	3.3375	2.2586	.5974	2.8666	2.2218
2.4449	1.9489	2.0704	6.4976	2.4449	1.9295	2.3000	4.2573	3.0058	1.4527
2.8233	.8138	2.2605	3.2074	2.8195	.8881	2.3546	3.0721	3.1978	1.1257
3.1959	.3416	2.4449	1.8940	3.2016	.3978	2.4468	2.1963	3.5799	.6641
3.4764	.1128	2.8195	.8632	3.4823	.1641	2.5447	1.7019	3.8585	.4564
3.7606	-.0551	3.1997	.3787	3.7625	.0017	2.6369	1.4515	4.1427	.3294
3.4801	.1089	3.4801	.1523	3.4839	.1631	2.8233	1.1181	3.8566	.4572
3.2072	.3263	3.7644	-.0128	3.1997	.3935	3.1997	.6700	3.5799	.6694
2.8254	.7972	3.4801	.1492	2.8233	.8754	3.5742	.4013	3.2072	1.1130
2.4468	1.9446	3.1997	.3758	2.4487	1.9396	3.8585	.2181	3.0209	1.4532
2.2680	3.1621	2.8233	.8410	2.2624	3.3838	4.1464	.0943	2.8666	2.2024
2.0779	6.2616	2.4487	1.8788	2.0610	7.1189	3.8679	.2137	2.6426	.0126
1.9179	13.7147	2.2624	3.3162	2.0026	9.6533	3.5818	.3971	2.4958	.0138
1.7899	.0180	2.0685	6.7361	1.9744	12.2518	3.1959	.6795	2.4751	.0145
1.5057	.0230	1.9292	10.6465	1.9518	10.2222	2.8214	1.1291	2.4487	.0147
		1.8822	.2172	1.9349	1.3550	2.4468	1.9644	2.2567	.0179
		1.6977	.0108	1.8784	.0575	2.2680	4.2900	2.0742	.0276
				1.6940	.0222	2.1043	.0205		
				1.5057	-.0176	1.8803	.0257		

TABLE II.- Concluded

(h) α = 40°; pitot-pressure probe

[h/l = 1.176]

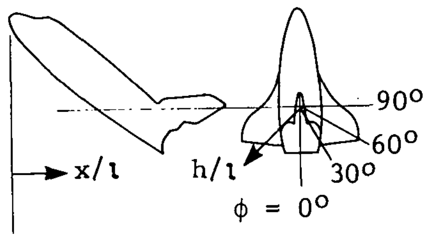

ϕ = 0°		ϕ = 8.5°		ϕ = 21.5°		ϕ = 38.5°		ϕ = 68.5°	
x/l	$\Delta p/p_\infty$	x/l	$\Delta p/p_\infty$	x/l	$\Delta p/p_\infty$	x/l	$\Delta p/p_\infty$	x/l	$\Delta p/p_\infty$
1.6958	0.0210	1.6921	0.0381	1.8521	0.0225	2.0647	0.0145	2.1664	0.0200
1.8784	.0109	1.9104	.0855	1.9085	.0145	2.1400	1.5230	2.3527	.0114
1.9198	1.7390	1.9349	4.6224	2.0083	3.9671	2.1457	3.3651	2.4129	.6869
1.9349	4.0731	1.9386	4.4385	2.0120	3.9207	2.1494	3.3533	2.4412	1.6192
1.9386	4.4670	2.0704	2.4970	2.0723	2.9956	2.1551	3.3476	2.4487	1.6487
1.9725	3.7351	2.2605	1.2567	2.2548	1.5103	2.1589	3.2423	2.4544	1.5829
2.0704	2.4884	2.4449	.5794	2.4449	.7734	2.1626	3.1722	2.5409	1.3308
2.2605	1.2631	2.8195	-.0442	2.8233	.0443	2.2454	2.4251	2.6369	1.0896
2.4449	.5795	3.2016	-.3300	3.1959	-.2110	2.2586	2.3209	2.8120	.7640
2.8195	-.0421	3.4820	-.4398	3.4764	-.3199	2.3000	2.0174	2.8609	.6936
3.1997	-.3432	3.7625	.5174	3.7606	-.4117	2.3546	1.7749	2.8666	.6964
3.4801	-.4619	3.4839	-.4407	3.4801	-.3210	2.4468	1.3963	3.0058	.5999
3.7644	-.5384	3.1997	-.3259	3.2072	-.2158	2.5447	1.0872	3.1978	.5257
3.4801	-.4624	2.8233	-.0415	2.8251	.0497	2.6369	.8468	3.5799	.2537
3.1997	-.3418	2.4487	.5822	2.4468	.7733	2.8233	.4483	3.8585	.1421
2.8233	-.0452	2.2624	1.2552	2.2680	1.4464	3.1997	.0428	4.1427	.0201
2.4487	.5809	2.0610	2.5494	2.0779	2.8866	3.5742	-.1400	3.8566	.1452
2.2624	1.2540	2.0026	3.2148	1.9179	.0002	3.8585	-.2347	3.5799	.2618
2.0685	2.4967	1.9744	3.7134	1.7899	.0160	4.1464	-.3057	3.2072	.5022
1.9292	2.6572	1.9518	4.0453	1.5057	.0436	3.8679	-.2328	3.0209	.5894
1.8822	-.0131	1.9349	4.2486			3.5818	-.1375	2.8666	.7040
1.6977	-.0009	1.8784	-.0112			3.1959	.0553	2.6426	1.0805
		1.6940	.0140			2.8214	.4659	2.4958	1.4529
		1.5057	-.0224			2.4468	1.2009	2.4751	1.5146
						2.2680	1.9695	2.4487	1.6014
						2.1043	3.2942	2.2567	-.0014
						1.8803	.0291	2.0742	.0224

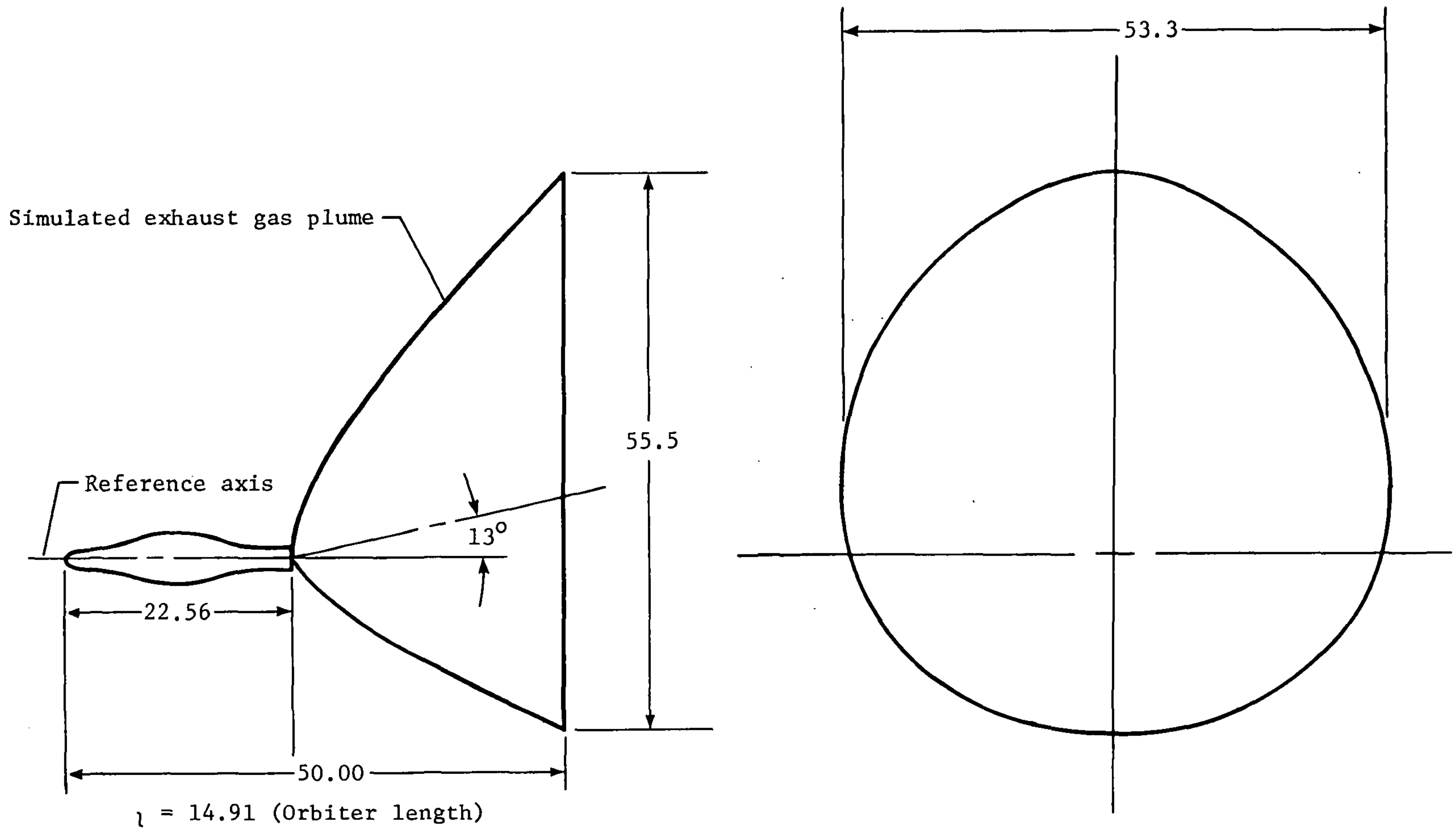

(a) 0.000456-scale model of equivalent body of revolution (orbiter and external fuel tank) with solid exhaust gas plume (Mach 6).

Figure 1.- Test models. All linear dimensions are in millimeters.

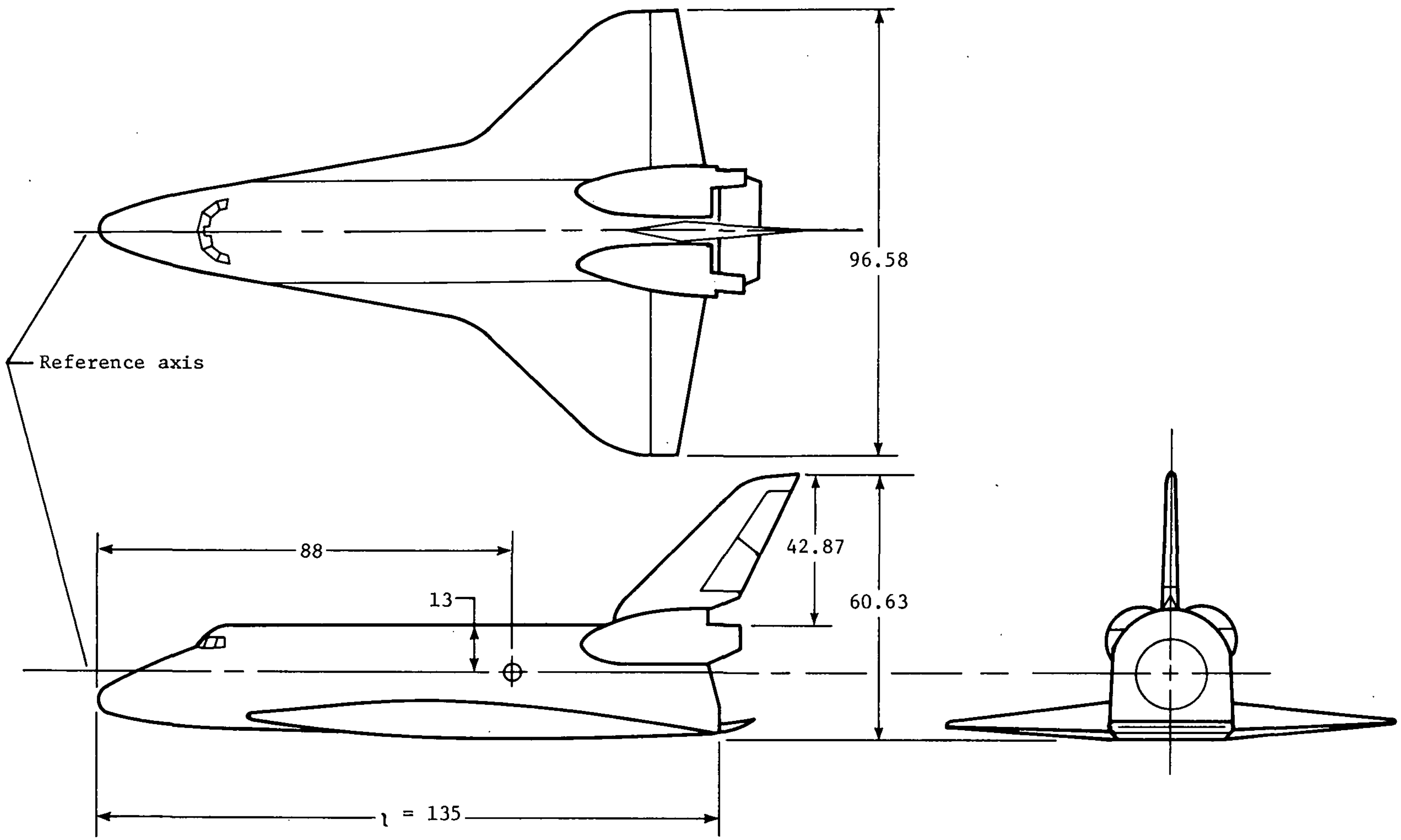

(b) 0.0041-scale model of 089B orbiter.

Figure 1.- Concluded.

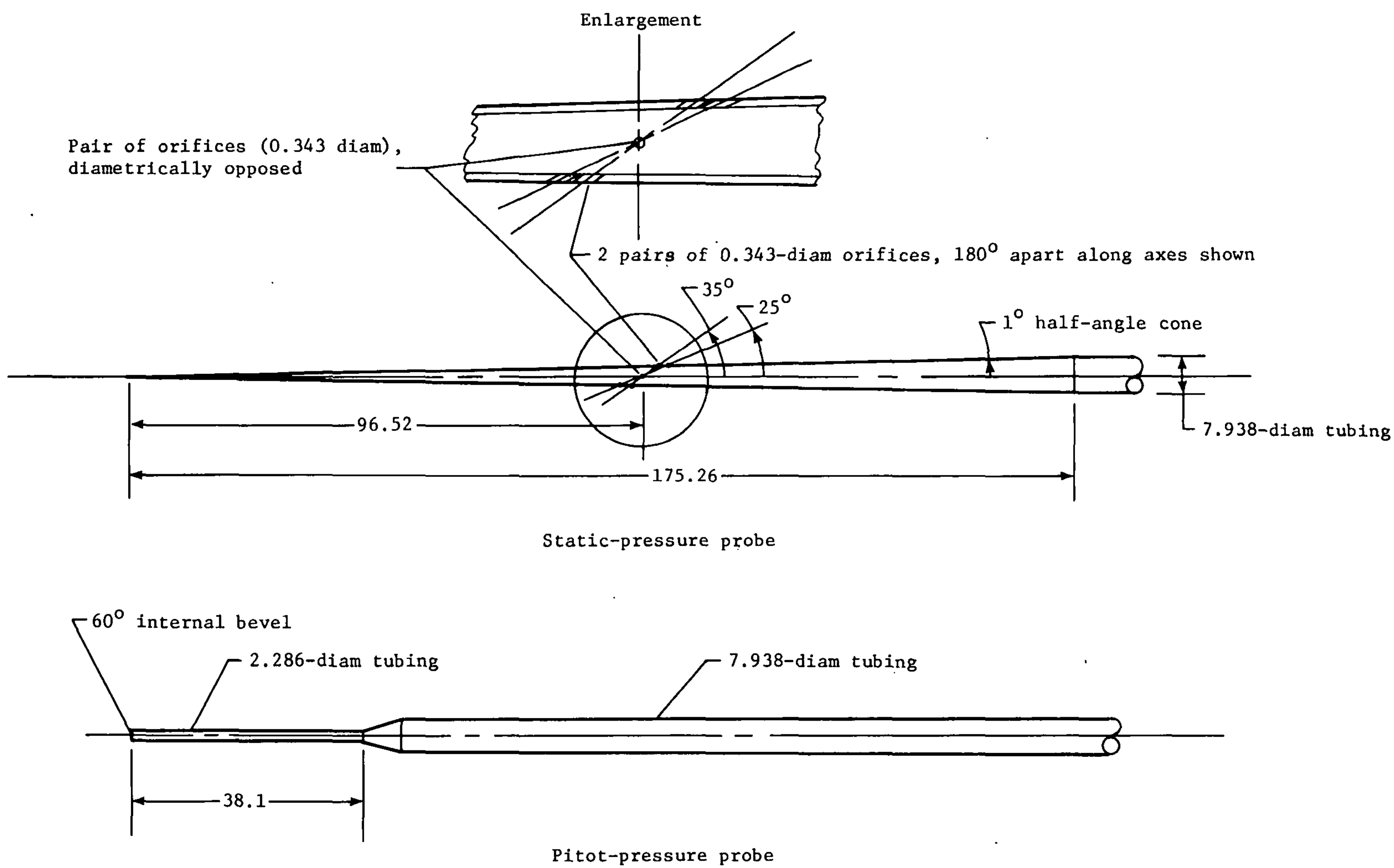

Figure 2.- Sketches of traverse probes. All linear dimensions are in millimeters.

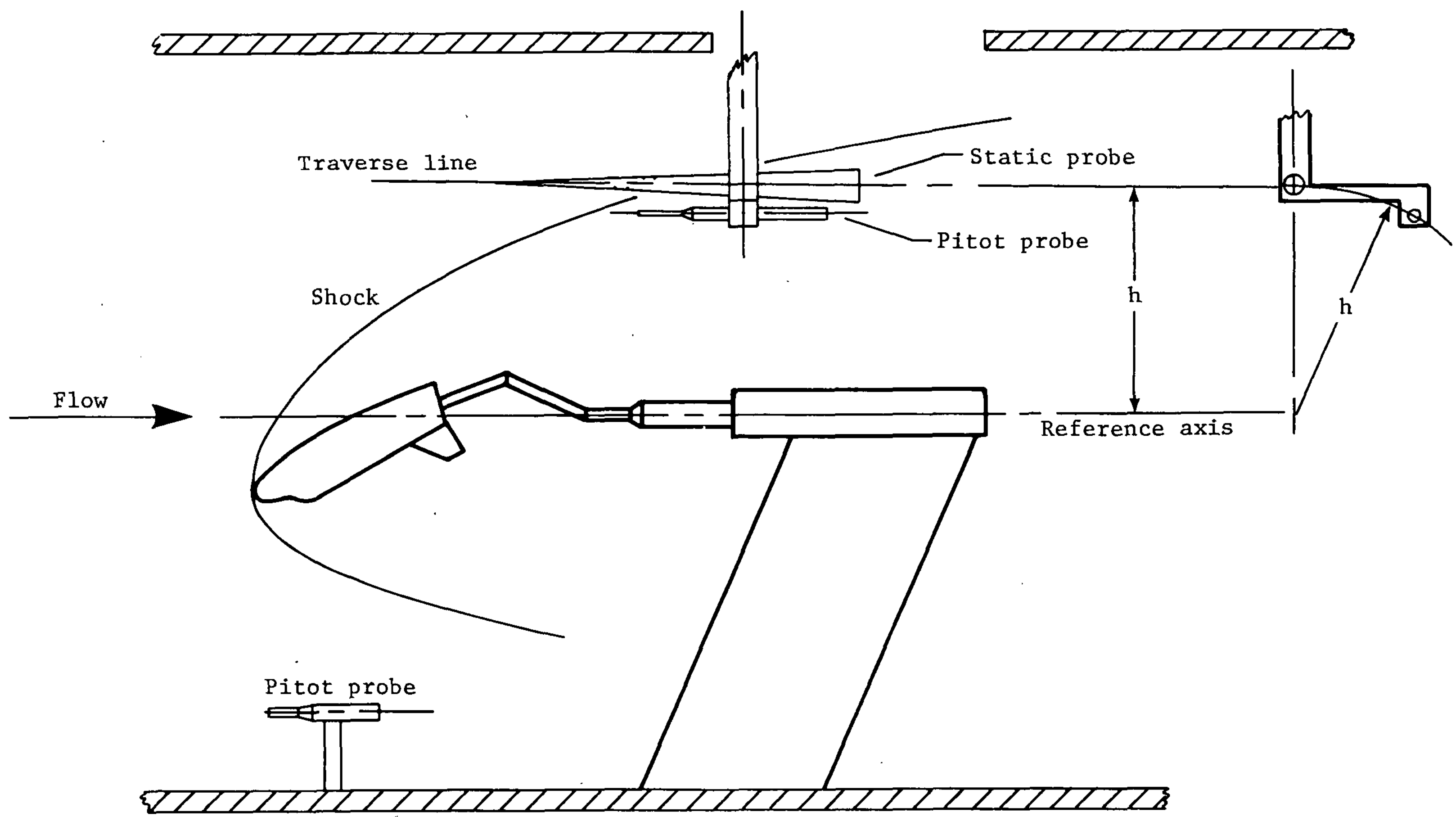

Figure 3.- Schematic of test setup.

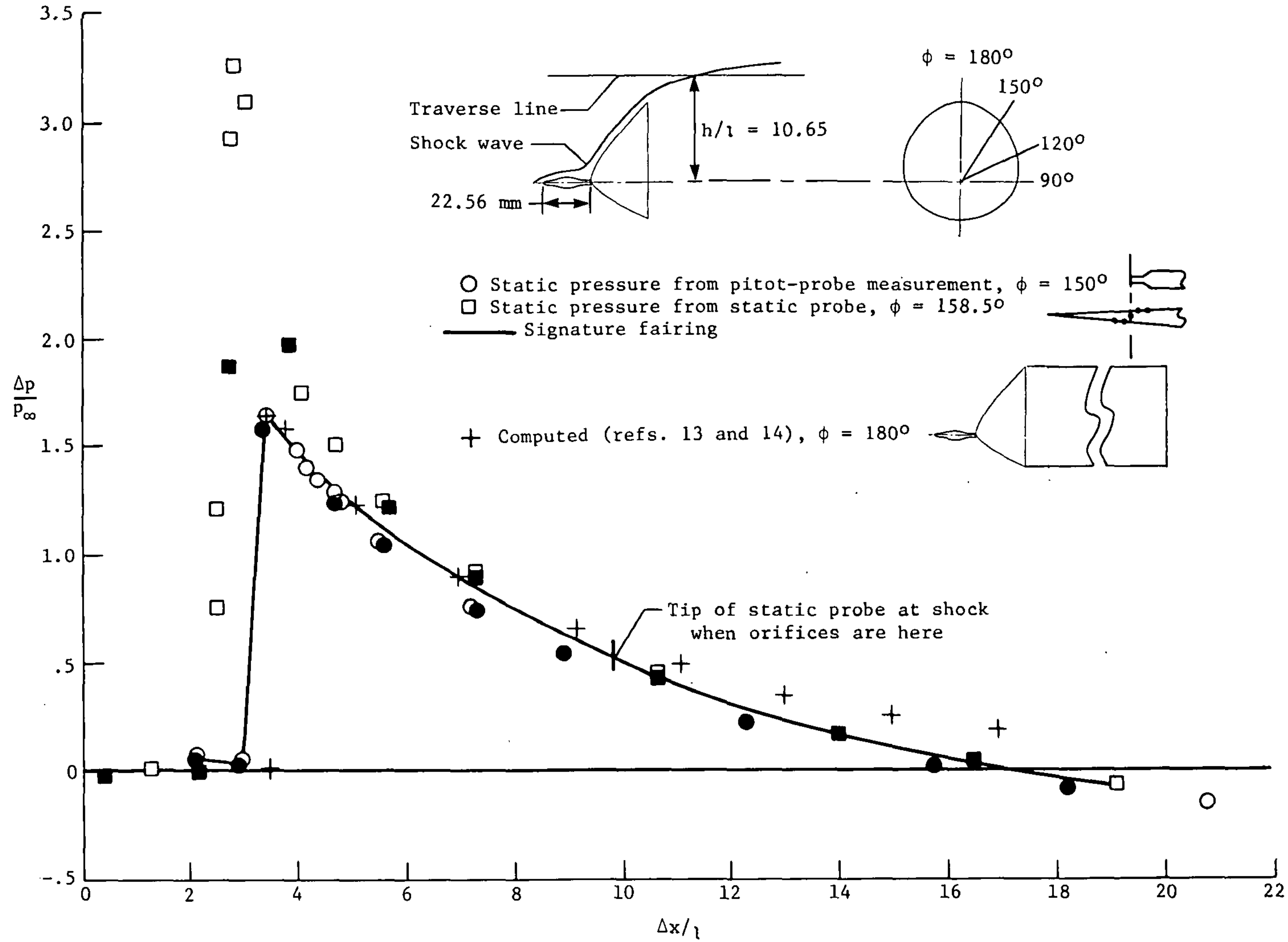

(a) $\phi = 150^{\circ}$.

Figure 4.- Pressure signatures for 0.000456-scale model of equivalent body of revolution (orbiter and external fuel tank) with solid exhaust gas plume (Mach 6) at two meridional angles. Filled symbols are from forward traverse. Origins were shifted for plotting. $\alpha = 0^{\circ}$.

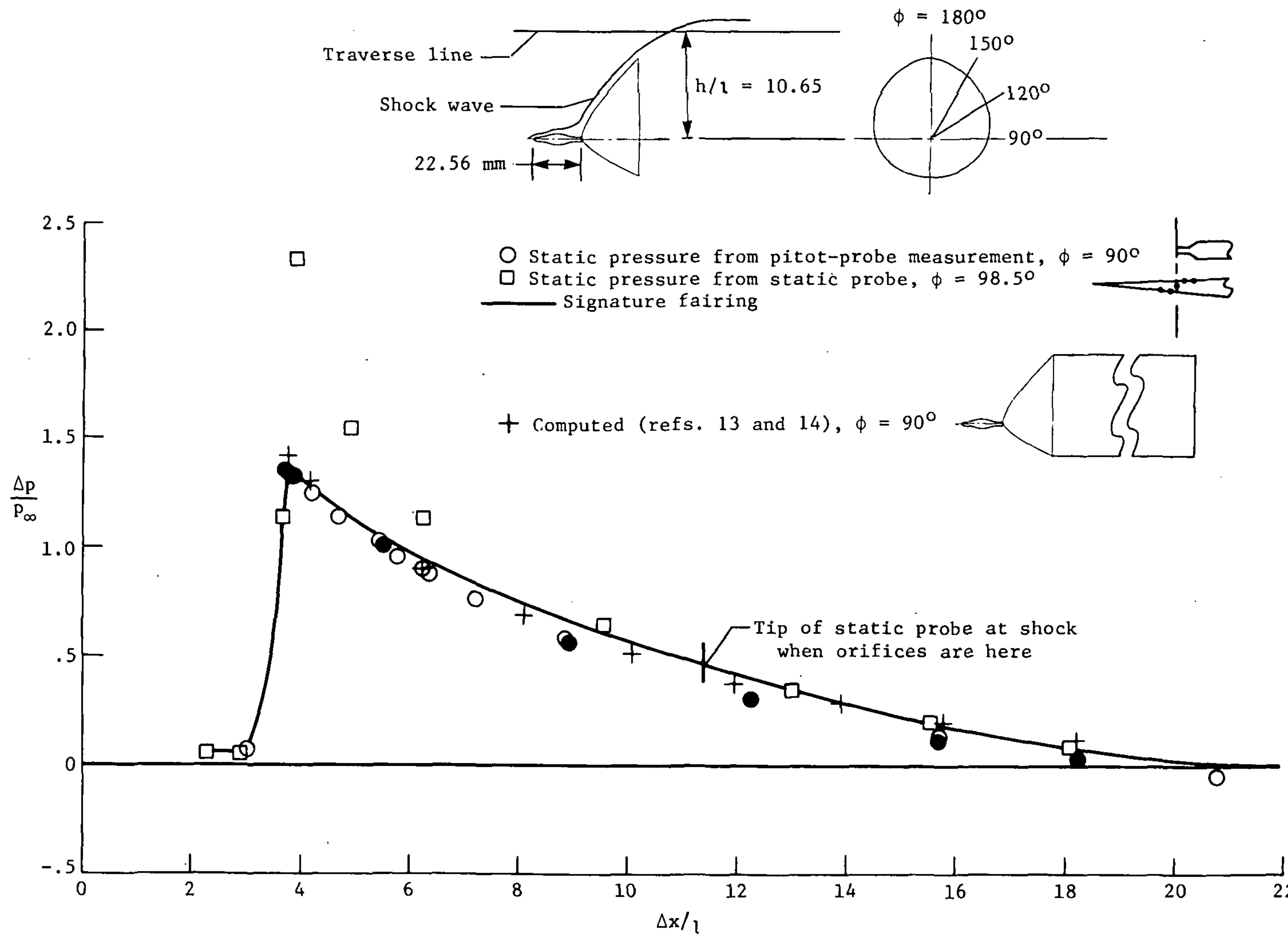

(b) $\phi = 90^{\circ}$.

Figure 4.- Concluded.

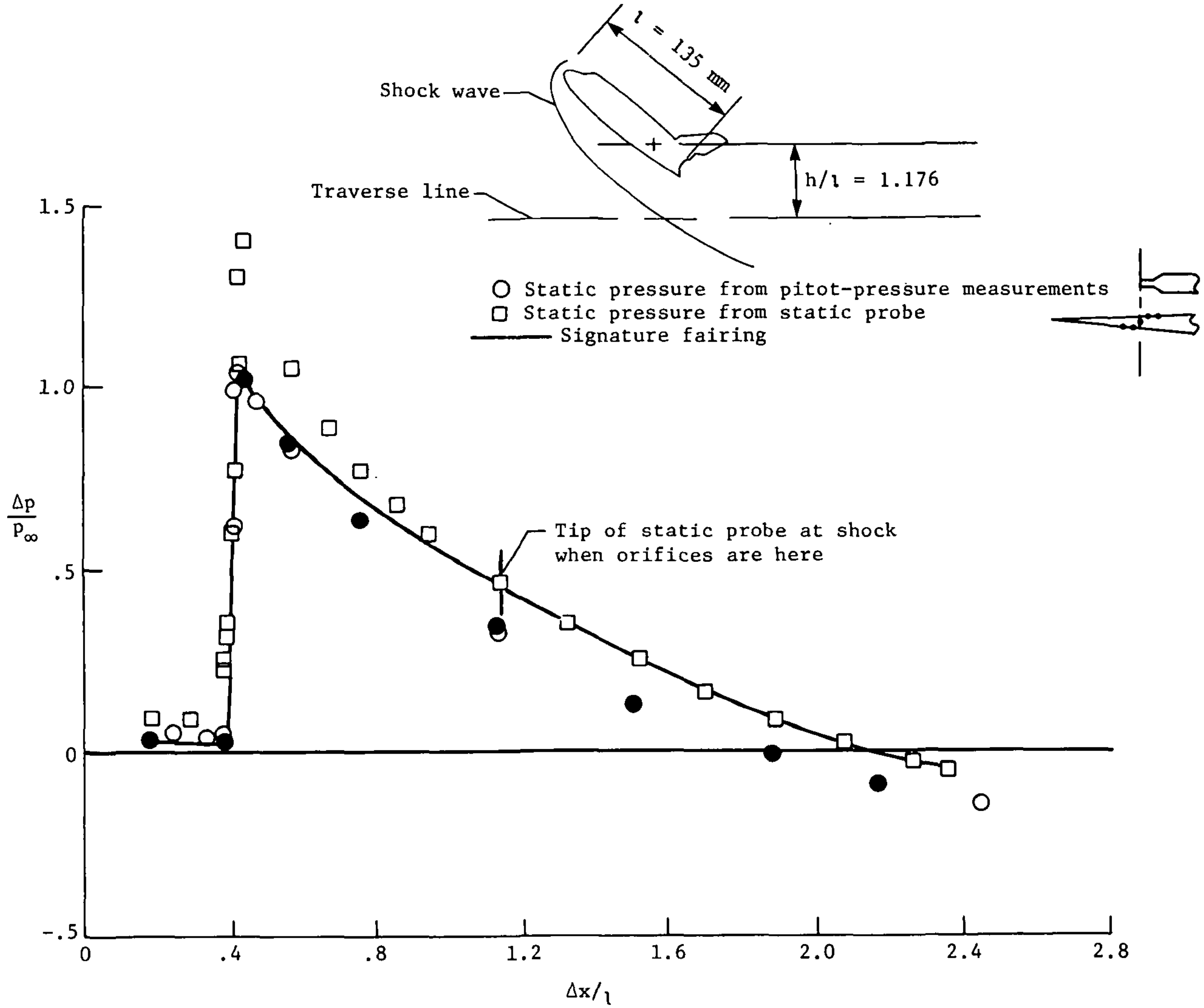

(a) $\alpha = 10^{\circ}$.

Figure 5.- Pressure signatures along plane of symmetry of 0.0041-scale model of the 089B orbiter at four angles of attack. Filled symbols are from forward traverse. Origins were shifted for plotting. $\phi = 0^{\circ}$.

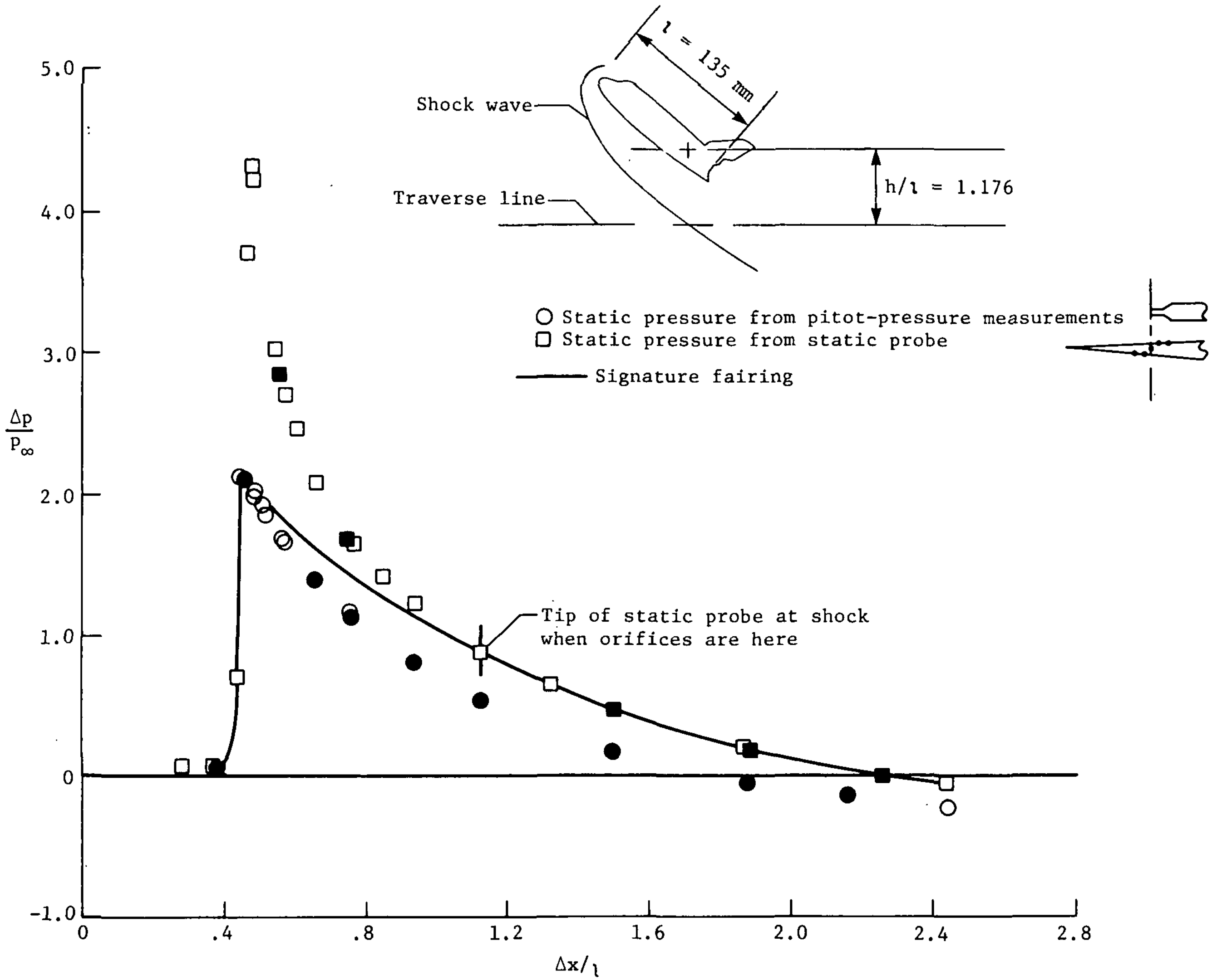

(b) $\alpha = 20^\circ$.

Figure 5.- Continued.

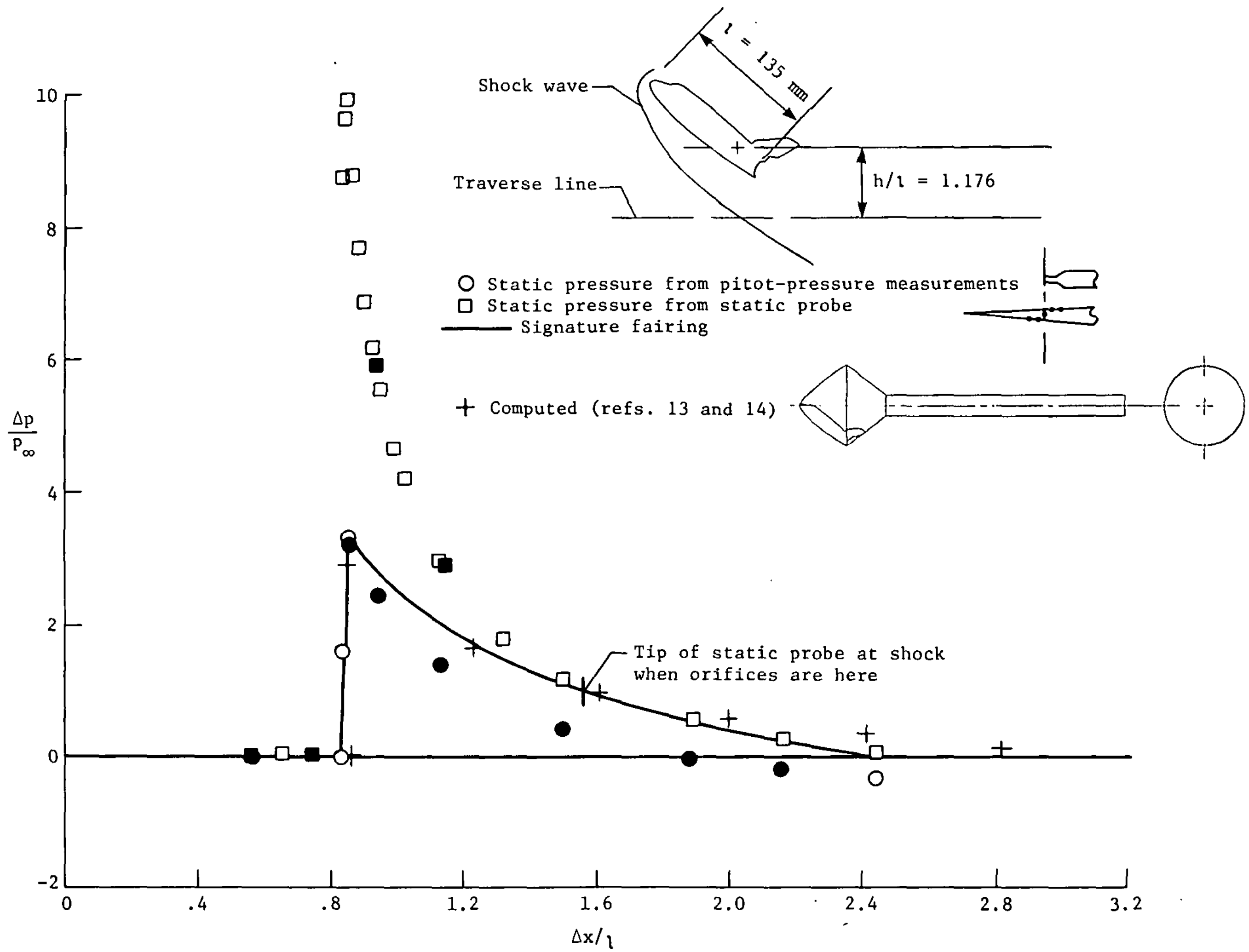

(c) $\alpha = 30^{\circ}$.

Figure 5.- Continued.

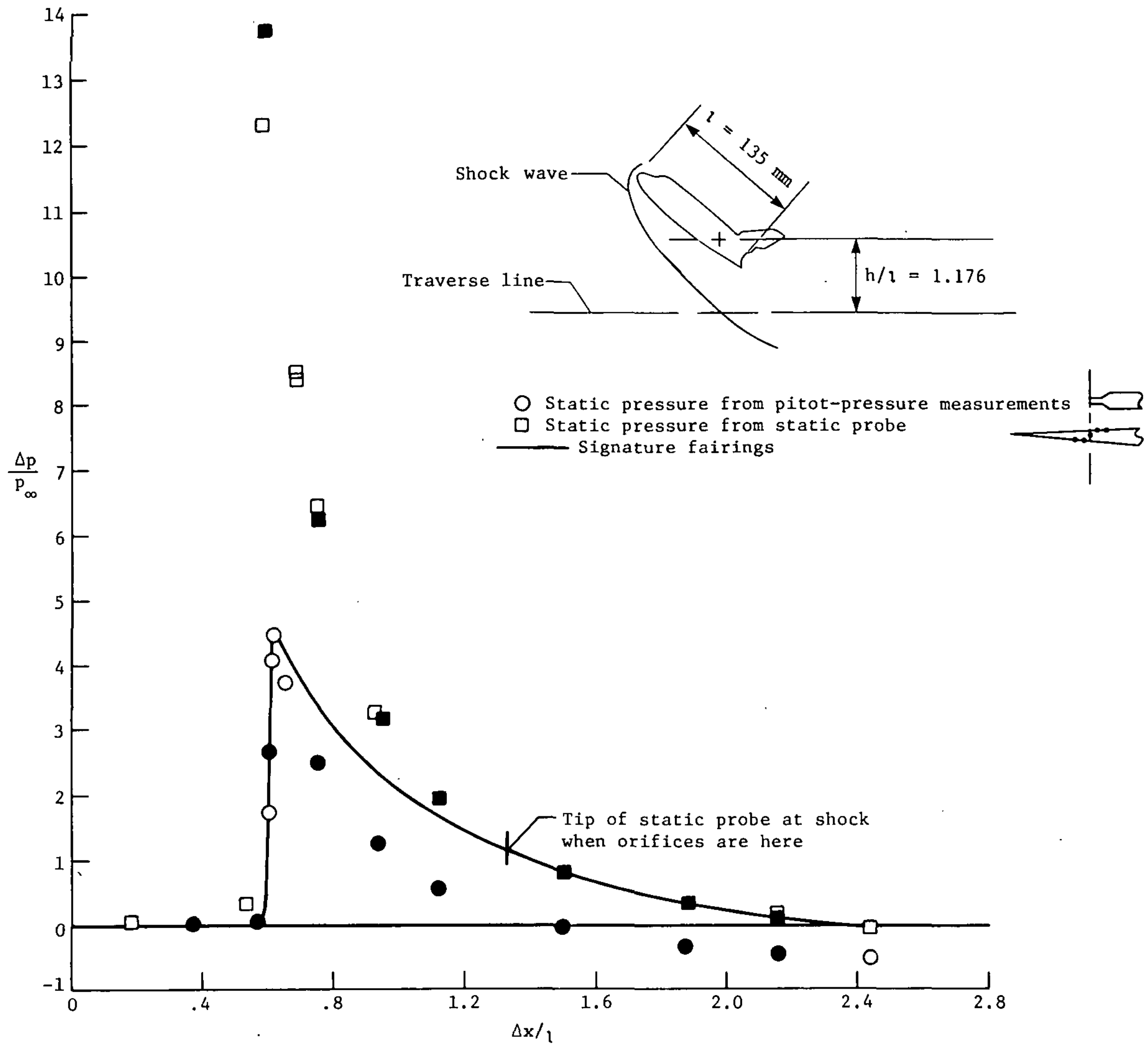

(d) $\alpha = 40^\circ$.

Figure 5.- Concluded.

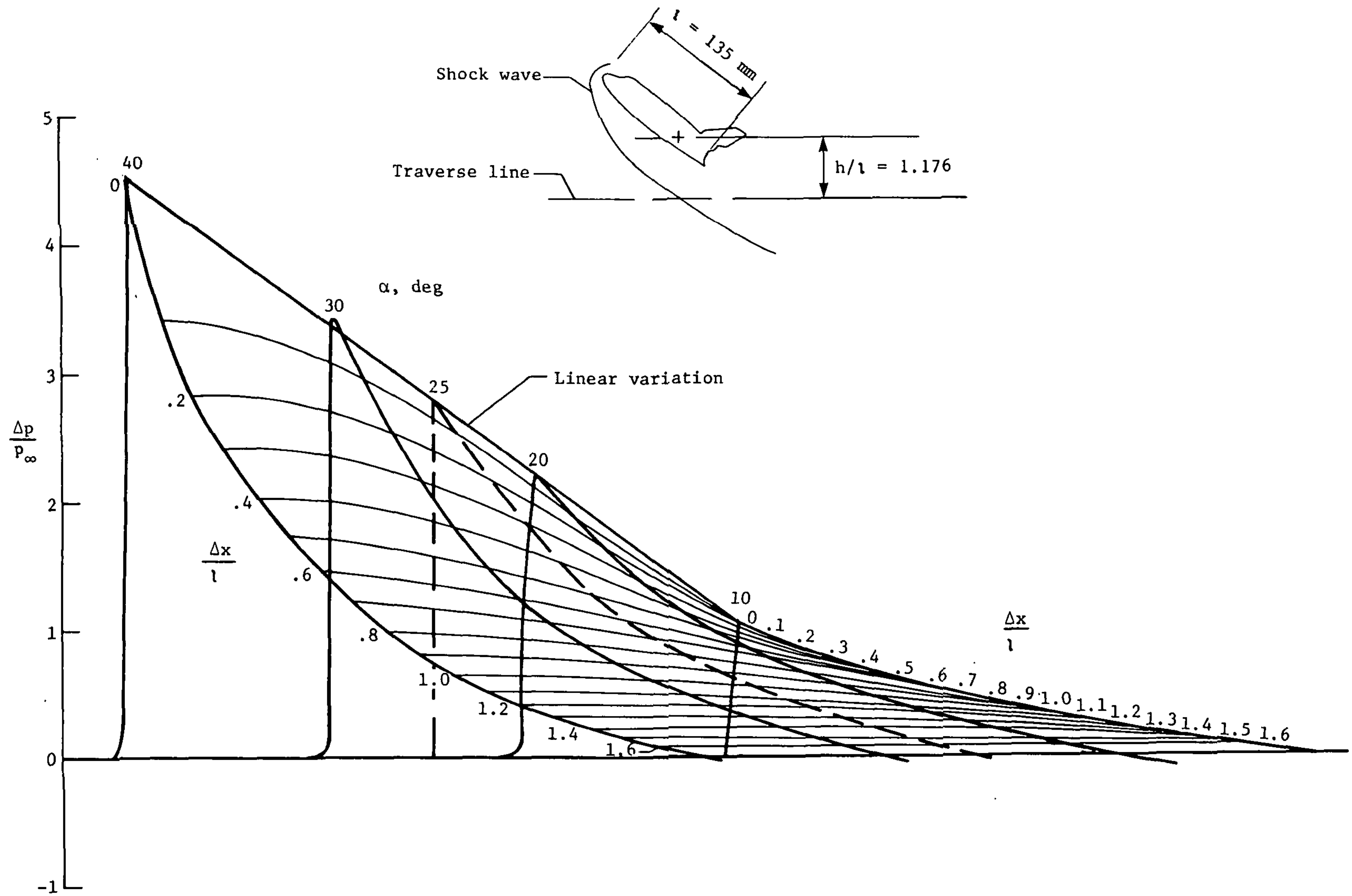

(a) Carpet plot of faired signatures at four angles of attack. Origins of signatures located at peak overpressures and plotted equidistance apart.

Figure 6.- Interpolation of pressure signature for $\alpha = 25^\circ$. $\phi = 0^\circ$.

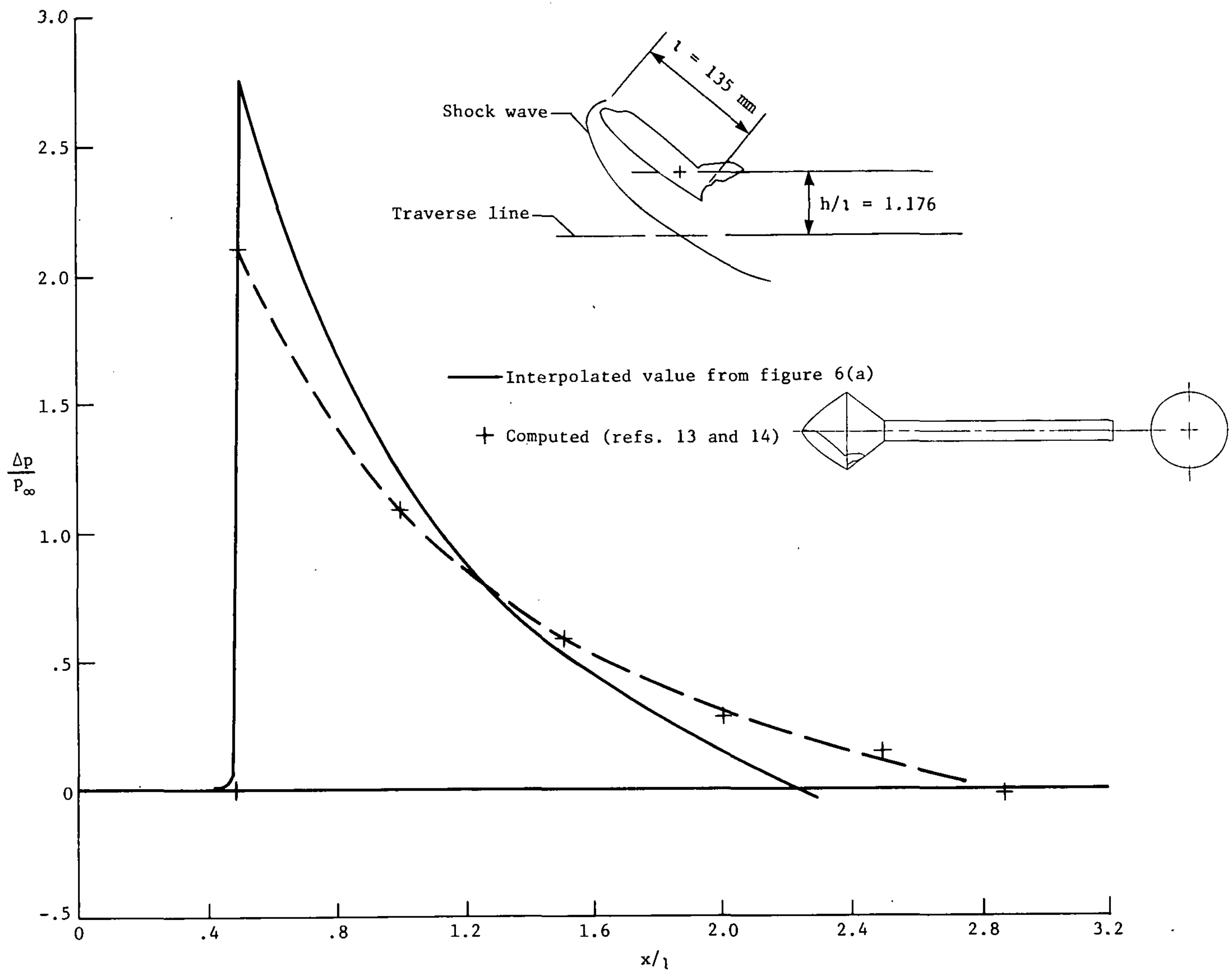

(b) Comparison of interpolated pressure signature from experiment with theoretical estimate. $\alpha = 25^{\circ}$.

Figure 6.- Concluded.

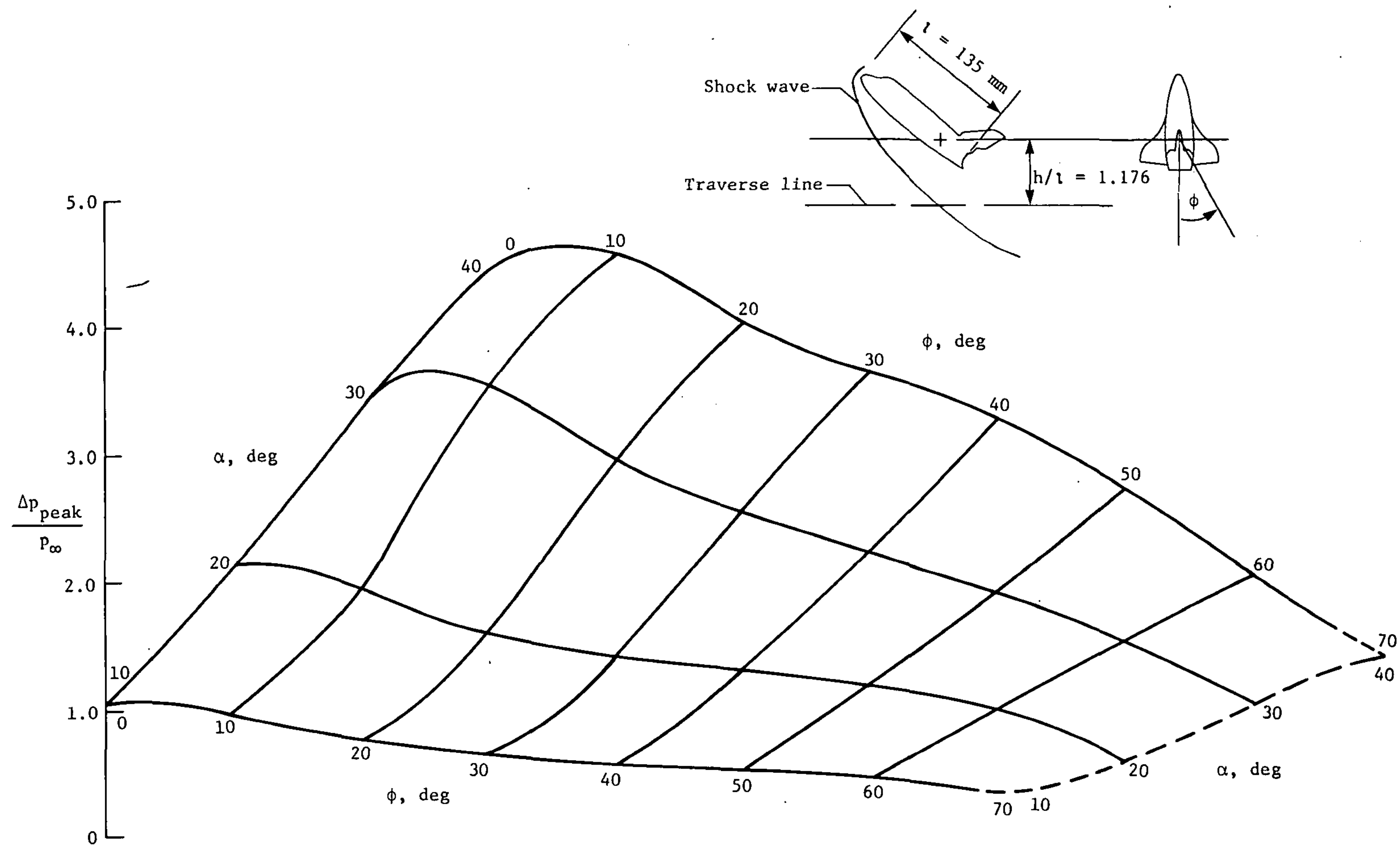

Figure 7.- Carpet plot of peak overpressures from pitot-pressure measurements at several meridional angles and angles of attack for the 089B orbiter.

1. Report No.	2. Government Accession No.	3. Recipient's Catalog No.
NASA TP-1405		

4. Title and Subtitle
NEAR-FIELD SONIC-BOOM PRESSURE SIGNATURES FOR THE SPACE SHUTTLE LAUNCH AND ORBITER VEHICLES AT MACH 6

5. Report Date
April 1979

6. Performing Organization Code

7. Author(s)
George C. Ashby, Jr.

8. Performing Organization Report No.
L-12638

9. Performing Organization Name and Address
NASA Langley Research Center
Hampton, VA 23665

10. Work Unit No.
506-26-33-03

11. Contract or Grant No.

12. Sponsoring Agency Name and Address
National Aeronautics and Space Administration
Washington, DC 20546

13. Type of Report and Period Covered
Technical Paper

14. Sponsoring Agency Code

15. Supplementary Notes

16. Abstract

Static-pressure signatures parallel to the flight path of the launch and entry configurations of the space shuttle have been measured in the Langley 20-inch Mach 6 tunnel in air at selected distances from the flight path. The launch configuration, consisting of an equivalent body of revolution (representing the orbiter and external fuel tank) with a solid exhaust gas plume attached, was tested at an angle of attack of 0°. The entry configuration (orbiter only) was tested over an angle-of-attack range from 10° to 40°. Calculated pressure signatures were in good agreement with measured signatures for both configurations.

17. Key Words (Suggested by Author(s))	18. Distribution Statement
Sonic boom Hypersonic Space shuttle	Unclassified - Unlimited Subject Category 16

19. Security Classif. (of this report)	20. Security Classif. (of this page)	21. No. of Pages	22. Price*
Unclassified	Unclassified	33	$4.50

* For sale by the National Technical Information Service, Springfield, Virginia 22161

NASA-Langley, 1979

National Aeronautics and
Space Administration

Washington, D.C.
20546

Official Business
Penalty for Private Use, $300

THIRD-CLASS BULK RATE

Postage and Fees Paid
National Aeronautics and
Space Administration
NASA-451

U.S.MAIL

NASA

POSTMASTER: If Undeliverable (Section 158 Postal Manual) Do Not Return